

Unveiling the progenitors of a population of likely peculiar GRBs

SI-YUAN ZHU ¹ AND PAK-HIN THOMAS TAM ¹

¹*School of Physics and Astronomy, Sun Yat-Sen University, Zhuhai 519082, People's Republic of China*

ABSTRACT

Traditionally, gamma-ray bursts (GRBs) are classified as long and short GRBs, with $T_{90} = 2$ s being the threshold duration. Generally, long-duration GRBs (LGRBs, $T_{90} > 2$ s) are associated with the collapse of massive stars, and short-duration (SGRBs, $T_{90} < 2$ s) are associated with the compact binary mergers involving at least one neutron star. However, the existence of a population of so-called “peculiar GRBs”, i.e., LGRBs originating from mergers, or long Type I GRBs, and SGRBs originating from collapsars, or short Type II GRBs, have challenged the traditional paradigm of GRB classification. Finding more peculiar GRBs may help to give us more insight into this issue. In this work, we analyze the properties of machine learning identified long Type I GRBs and short Type II GRBs candidates, long GRBs-I and short GRBs-II (the so-called “peculiar GRBs”). We find that long GRBs-I almost always exhibit properties similar to Type I, which suggests that the merger may indeed produce GRBs with $T_{90} > 2$ s. Furthermore, according to the probability given by the redshift distribution, short GRBs-II almost exhibit properties similar to Type II. This suggests that the populations of short Type II GRBs are not scarce and that they are hidden in a large number of samples without redshifts, which is unfavorable to the interpretation that the jet progression leads to a missed main emission.

Keywords: gamma-ray burst: general – methods: data analysis

1. INTRODUCTION

Gamma-ray bursts (GRBs) are the brightest electromagnetic explosions in the universe. Theoretically, the merger of compact binaries (Type I GRB) and the collapsar of massive stars (Type II GRBs) will produce GRBs (Paczynski 1986; Woosley 1993; Zhang et al. 2007, 2009). According to the collapsar scenario, the duration of GRBs is defined by the envelope fallback timescale, typically 10 s (MacFadyen & Woosley 1999). Furthermore, the timescale of GRBs originating from neutron star–neutron star (NS–NS) and neutron star–black hole (NS–BH) mergers typically is 0.01–0.1 s, which suggests that merged GRBs should typically have short durations (Aloy et al. 2005).

According to the bimodal distribution of durations, GRBs are directly classified into long GRBs (LGRBs, $T_{90} > 2$ s) and short GRBs (SGRBs, $T_{90} < 2$ s) (Kouveliotou et al. 1993), where T_{90} is time interval with integrated photon counts raise from 5% to 95%. Previously, observations have revealed that LGRBs are asso-

ciated with supernovae (SNe) originating from massive collapsars (such as GRB 030329/SN 2003dh) (Stanek et al. 2003), and SGRBs are associated with gravitational waves (GWs) and kilonova (KNe) both originating from compact binary mergers (such as GRB 170817A/GW170817) (Abbott et al. 2017a,b; Wang et al. 2017).

GRBs originating from different progenitors exhibit distinct observational properties. Spectral lag (τ) is defined as the time delay of high-energy photons with respect to low-energy photons (Norris et al. 1986; Cheng et al. 1995). Generally, LGRBs have significant τ , while SGRBs have negligible or tiny τ (Yi et al. 2006; Bernardini et al. 2015). Furthermore, Amati et al. (2002) analyzed 10 LGRBs with known redshift (z) and first found a tight correlation between the rest frame peak energy ($E_{p,z}$) in the νf_ν spectrum and isotropic energy (E_{iso}), the $E_{p,z}$ – E_{iso} correlation. LGRBs and SGRBs follow different $E_{p,z}$ – E_{iso} correlation, and exhibit significant separation in the $E_{p,z}$ – E_{iso} plane (Qin & Chen 2013; Minaev & Pozanenko 2020; Li et al. 2023; Zhu et al. 2023).

However, recent observations suggest that the dichotomy based on phenomenological does not necessarily correspond to the two progenitors of GRBs. GRB

211211A is a LGRB with $T_{90} \sim 34$ s. Its lightcurve of whole emission (WE) is characterized by an initial short-hard spiky main emission (ME) followed by a long-soft extended emission (EE), similar to some SGRBs with EE associated with KNe (Jin et al. 2016; Gao et al. 2017). In addition, Its optical and near-infrared transients that emerged after the burst were similar to KN after GW170817, which suggests that it is a Type I GRB (Rastinejad et al. 2022; Troja et al. 2022; Yang et al. 2022). Yang et al. (2022) calculated τ of both ME and EE and found their tiny τ is consistent with typical SGRBs. In the $E_{p,z}-E_{\text{iso}}$ plane, ME follows the track of SGRBs, while EE and WE do not (Yang et al. 2022). Although the WE duration is mostly contributed by EE for GRB 211211A, the ME duration (~ 13 s) is still too long for merger scenario. The neutron star–white dwarf (NS–WD) merger was suggested as an explanation that theoretically allows it to produce long duration GRBs (King et al. 2007; Yang et al. 2022; Zhong et al. 2023). However, the collapsar origin has not been ruled out (Barnes & Metzger 2023).

GRB 200826A is a SGRB with $T_{90} \sim 1$ s but associated with a SN, suggesting it is a Type II GRB (Ahumada et al. 2021; Zhang et al. 2021; Rossi et al. 2022). Zhang et al. (2021) calculated the energy-dependent τ between the lowest energy (10–20 keV) band and any higher energy band. It has a maximum τ of 157 ± 51 ms, which is consistent with typical LGRBs. GRB 200826A also follow the $E_{p,z}-E_{\text{iso}}$ track of LGRBs. However, its duration is much shorter than the timescale of collapsar scenarios. Missing the ME phase because of geometric effects caused either by jet precession or companion obstruction models has been proposed to explain GRB 200826A while putting forward a high demand on the rarity of SGRBs originating from collapsars (Wang et al. 2022).

Besides the above, some SGRBs (such as GRB 090426 and GRB 100816A) are thought to possibly originate from collapsars (Zhang et al. 2009; Fan & Wei 2011; Nicuesa Guelbenzu et al. 2011; Xin et al. 2011; Zhang et al. 2012), as well as some LGRBs (such as GRB 060614 and GRB 230307A) are thought to possibly originate from mergers (Della Valle et al. 2006; Fynbo et al. 2006; Gal-Yam et al. 2006; Gehrels et al. 2006; Levan et al. 2024; Yang et al. 2024). They have broken the correspondence between the duration of GRBs and their progenitors. According to the different observational properties, Zhang et al. (2009) proposed that GRBs can be classified based on multiband observation. However, most GRBs cannot be accurately located and follow observation limited by observation. The contradiction between observation and theory on timescales has not been

resolved. Additional long Type I GRBs and short Type II GRBs are required to support that they are the tail of T_{90} distribution or the result of some special physical process.

Machine learning has been widely used to classify GRBs based solely on lightcurves or physical parameters of the prompt emission (γ -ray) (Jespersen et al. 2020; Bhardwaj et al. 2023; Dimple et al. 2023; Steinhardt et al. 2023; Chen et al. 2024; Zhu et al. 2024). The unsupervised dimensionality reduction algorithm, t-distributed stochastic neighbor embedding (t-SNE) (Maaten & Hinton 2008; Maaten 2014) and Uniform Manifold Approximation and Projection (UMAP) (McInnes et al. 2018), can reduce adjacent datapoints in high-dimensional space to adjacent points in a two-dimensional space without prior for partial burst classification. Zhu et al. (2024) applied the t-SNE and UMAP to the Fermi Catalog and found two clusters with a clear separation in the t-SNE and UMAP maps, GRBs-I (may correspond to Type I GRBs) and GRBs-II (may correspond to Type II GRBs). Interestingly, the distribution of these two types overlaps in T_{90} . With a boundary of 2 s, there are some long GRBs-I and short GRBs-II that may correspond to long Type I GRBs and short Type II GRBs, respectively, which are peculiar GRBs. In the peculiar GRBs, GRB 200826A is classified as GRBs-II along with the typical Type II GRBs, which supports the machine learning classification method that short GRBs-II originate from collapsars and long GRBs-I originate from mergers. Unfortunately, the progenitor of remaining long GRBs-I and short GRBs-II cannot be identified due to the lack of associated SNe/KNe observations.

In this work, we aim to determine the progenitors of long GRBs-I and short GRBs-II by studying the variation of their properties with redshift, since most of them have no observed redshift. The structure of our article is organized as follows. In Section 2, we describe the sample selection criteria and data analysis. The properties of the long GRBs-I and short GRBs-II are shown in Section 3. The discussions are shown in Section 4. The conclusions are shown in Section 5.

2. SAMPLE SELECTION AND DATA ANALYSIS

In order to investigate the detailed properties of GRBs, accurate spectral parameters are crucial. The Fermi Gamma-ray Burst Monitor (GBM) detector with the broad energy band (8 keV–40 MeV) has enriched the sample of GRBs with reliable E_p (Meegan et al. 2009). The Fermi GRBs are taken from the Fermi Cat-

alog¹ until the end of April 2023 (von Kienlin et al. 2020). We mainly consider GRBs with a well-measured spectrum. The four spectral models including the Band model (Band et al. 1993), the power law (PL) model, the cutoff power law (CPL) model, and the smoothly broken power law (SBPL) model are used to fit the spectra of GRBs. The values of the spectral parameter and fluence (S_γ) are mainly taken from the best spectral fitting model, which is obtained directly from the Fermi Catalog. If the best fitting model of one GRB is the PL model, we take the CPL model to get the spectrum parameter and S_γ . To ensure the accuracy of E_p , we exclude the GRBs in which the error of E_p is larger than 40%. To eliminate the effect of the time resolution on the peak flux (F_p), we uniformly select the F_p with the timescale of 64 ms for all GRBs. A total of 2057 GRBs are selected. In order to better identify the progenitors of peculiar GRBs, we add 32 GRBs with SN signals, 7 GRBs with KNe signals (the MEs of GRB 060614, GRB 211211A, and GRB 211227A are recorded as a separate sample), and one GRB may originating from magnetar giant flare (MGF), a total of 40 GRBs. Finally, we compiled a sample containing 2097 GRBs, some observation data of GRBs with redshift are listed in Table 1.

Zhu et al. (2024) discovered 42 long GRBs-I and 14 short GRBs-II from the Fermi Catalog through UMAP and discovered 47 long GRBs-I and 14 short GRBs-II from the Fermi Catalog through t-SNE. We compiled these GRBs as the peculiar sample, a total of 61 GRBs, and divided them into four groups, the details of which are listed in Table 2. Group A contains 41 LGRBs classified as long GRBs-I by both t-SNE and UMAP. Group B contains 13 SGRBs classified as short GRBs-II by both t-SNE and UMAP. GRB 200826A was not included in Group B for further analysis since its progenitors were known. Group C contains 6 GRBs classified as long GRBs-I by t-SNE but they are classified as GRBs-II by UMAP. Group D contains 1 SGRB classified as short GRBs-II by t-SNE but they are classified as GRBs-I by UMAP.

The hardness ratio (HR, defined as the ratio of the observed counts of high-energy photons to the low-energy photons) of Fermi GRBs that are calculated by the ratio of the observed counts (background subtraction) in the energy range of 50–300 and 10–50 keV from von Kienlin et al. (2020), except for one of the negative values. We downloaded the GBM time-tagged event (TTE) data of long GRBs-I and short GRBs-II from Fermi Archive

FTP websites². The TTE data from all triggered NaI detectors were used in our analysis. The lightcurves were extracted with the standard Fermi tool for python source *GBM Data Tools*.

In order to explore the physical properties of GRB in the rest frame, we compiled a GRB sample with redshift and listed in Table 1, a total of 153 GRBs. Then we estimated the rest frame parameters of the GRB sample with redshift. In this paper, both E_{iso} and L_{iso} are corrected to the energy band of 1–10⁴ keV in the rest frame. The E_{iso} is calculated by

$$E_{\text{iso}} = \frac{4\pi D_L^2 S_\gamma k}{(1+z)}, \quad (1)$$

where D_L is the luminosity distance, S_γ is the fluence, and k is the k -correction factor. In this paper, we assume a flat universe ($\Omega_k = 0$) with the cosmological parameters $H_0 = 71 \text{ km s}^{-1} \text{ Mpc}^{-1}$, $\Omega_M = 0.27$, and $\Omega_\Lambda = 0.73$. The correction factor k is defined as

$$k = \frac{\int_{1/(1+z)}^{10^4/(1+z)} EN(E)dE}{\int_{e_{\text{min}}}^{e_{\text{max}}} EN(E)dE}, \quad (2)$$

where e_{min} and e_{max} are the observational energy band of fluence, $N(E)$ denotes the photon spectrum of GRB (Schaefer 2007). The best fitting spectral model for $N(E)$ is selected. The isotropic luminosity L_{iso} is calculated by

$$L_{\text{iso}} = 4\pi D_L^2 F_p k, \quad (3)$$

where F_p is the peak flux, in units of $\text{erg cm}^{-2} \text{ s}^{-1}$. When GRBs with photon peak flux P_p (in units of $\text{photon cm}^{-2} \text{ s}^{-1}$), F_p is calculated by:

$$F_p = P_p \frac{\int_{e_{\text{min}}}^{e_{\text{max}}} EN(E)dE}{\int_{e_{\text{min}}}^{e_{\text{max}}} N(E)dE}. \quad (4)$$

The rest frame peak energy $E_{p,z}$ and duration $T_{90,z}$ are calculated as $E_{p,z} = E_p(1+z)$ and $T_{90,z} = T_{90}/(1+z)$, respectively. The symbolic notation $Q_n = Q/10^n$ is adopted.

3. PROPERTIES OF THE LONG GRBS-I AND SHORT GRBS-II

3.1. Spectral Hardness

Spectral hardness can usually be represented by HR , the low-energy spectral index (α), and E_p . Generally, SGRBs are harder than LGRBs. SGRBs and LGRBs are clustered in distinct regions in the HR - T_{90} , the α - T_{90} , and the E_p - T_{90} planes (Zhang et al. 2012).

¹ <https://heasarc.gsfc.nasa.gov/W3Browse/fermi/fermigbrst.html>

² <https://heasarc.gsfc.nasa.gov/FTP/fermi/data/gbm>

In both the E_p-T_{90} and the $HR-T_{90}$ planes, GRBs of our sample are clustered in distinct regions, as shown in Figure 1. We use the Gaussian mixture model (GMM) to divide the GRBs into LGRBs and SGRBs and given the probability that each GRB is classified as a LGRB (Tsutsui & Shigeyama 2014; Zhang et al. 2016). The probabilities of the peculiar GRB samples are listed in Table 2.

For Group A, only GRB 080828189 and GRB 081006604 are classified as LGRBs in the E_p-T_{90} plane with 80.97% and 62.31% probability, respectively, and 9 GRBs (including GRB 081006604) are classified as LGRBs in the $HR-T_{90}$ plane with less than 90% probability. Only four GRBs, GRB 081107321, GRB 100816026 (or, GRB 100816A), GRB 171126235, and GRB 180511437 in Group B are classified as LGRBs in the E_p-T_{90} plane with less than 65% probability, and all are classified as SGRBs in the $HR-T_{90}$ plane. GRB 090320045 and GRB 140912664 in Group C are classified as SGRBs in the E_p-T_{90} plane, and except for GRB 101002279 and GRB 120504945, they are all classified as SGRBs in the $HR-T_{90}$ plane. Group D is classified as SGRBs by different planes.

In addition, some studies have found that MGFs, if occurring in nearby galaxies, would appear as cosmic short-hard GRBs (Yang et al. 2020; Zhang et al. 2020; Roberts et al. 2021; Svinkin et al. 2021; Mereghetti et al. 2024; Trigg et al. 2024; Yin et al. 2024). The lightcurves and spectrum of MGFs are not significantly different from classical SGRBs. Compelling evidence for period-modulated tail induced by the magnetar rotation cannot be observed by current wide-field gamma-ray monitors (Svinkin et al. 2021). Thus, the main evidence for distinguishing MGFs from SGRBs is the spatial coincidence with nearby galaxies and the consistency of the energetics with known MGFs. When they cannot be localized, the rapid rise in the lightcurve, duration on the order of milliseconds, and very short time variability are possible clues, but not unique (Trigg et al. 2024). We will consider the possibility that MGFs serve as progenitors of peculiar GRBs. In our sample, three GRBs are considered as MGF candidates, GRB 180128A, GRB 200415A, and GRB 231115A. They are classified as SGRBs in both the E_p-T_{90} and the $HR-T_{90}$ planes and do not show special features.

3.2. The $E_{p,z}-E_{\text{iso}}$ plane

Since the $E_{p,z}-E_{\text{iso}}$ correlation was discovered by Amati et al. (2002), classification of GRBs based on the $E_{p,z}-E_{\text{iso}}$ plane have been widely studied.

3.2.1. The $E_{p,z}-E_{\text{iso}}$ correlation

The $E_{p,z}-E_{\text{iso}}$ correlation have been widely discussed as a GRB classifier (Zhang et al. 2012; Qin & Chen 2013; Zhang et al. 2020; Amati 2021; Zhang et al. 2021; Yang et al. 2022; Zhu et al. 2022, 2023). Recent studies have confirmed that the Type I GRBs and the Type II GRBs follow different $E_{p,z}-E_{\text{iso}}$ correlations, and exhibit significant separation in the $E_{p,z}-E_{\text{iso}}$ plane, whereas some low-luminosity LGRBs (LL-LGRBs) are inconsistent with the $E_{p,z}-E_{\text{iso}}$ correlation of Type II GRBs (Amati 2006; Zhang et al. 2018; Minaev & Pozanenko 2020; Li et al. 2023; Zhu et al. 2023).

Almost all of the peculiar GRBs in our sample are without redshift, so we simulate $E_{p,z}$ and E_{iso} for peculiar GRBs at redshifts from 0.0001 to 10, the redshift evolution trajectories are shown in Figure 2. We can see that Group A GRBs and Group B GRBs are significantly different from the trajectories of LGRBs and SGRBs in the $E_{p,z}-E_{\text{iso}}$ plane. Apart from GRB 080828189 and GRB 161001045 (or, GRB 161001A), whose trajectories slightly cross the 2σ prediction interval boundary of the $E_{p,z}-E_{\text{iso}}$ correlation for LGRBs, all of the remaining Group A GRBs are above this boundary, which is clearly different from other LGRBs. However, the redshifts of GRB 161001045 and GRB 180618030 (or, GRB 180618A) are 0.67 and 0.544, respectively. Their confirmed $E_{p,z}$ and E_{iso} indicate that they are both outliers above the 2σ prediction interval of LGRBs (Fong et al. 2022; Jordana-Mitjans et al. 2022). Group B GRBs enter the 2σ prediction interval of LGRBs as the redshift becomes larger, and are within the 2σ prediction interval over a wide range. Among them, GRB 100816026 has $z = 0.805$ and follows the track of the $E_{p,z}-E_{\text{iso}}$ correlation of LGRBs. Group C GRBs are all above the 2σ prediction interval except for GRB 081130212 and GRB 131128629, which are within the 2σ prediction interval in the large redshift range. Group D GRBs are within the 2σ prediction interval in the few redshift range.

The MGFs are located in the upper left corner of the $E_{p,z}-E_{\text{iso}}$ plane, and their tracks with redshift in the $E_{p,z}-E_{\text{iso}}$ plane are not significantly different from the SGRBs. This indicates that if the distance or redshift of the SGRBs cannot be determined, MGFs can hardly be recognized.

3.2.2. ε and EHD parameter

According to the significant separation in the $E_{p,z}-E_{\text{iso}}$ plane, Lü et al. (2010) and Minaev & Pozanenko (2020) proposed two similar parameters to classify GRBs, $\varepsilon = (E_{\text{iso}}/10^{52})/(E_{p,z}/100)^{5/3}$ and the energy-hardness $EH = (E_{p,z}/100)/(E_{\text{iso}}/10^{51})^{0.4}$, respectively. Lü et al. (2010) suggested that the Type I GRBs have

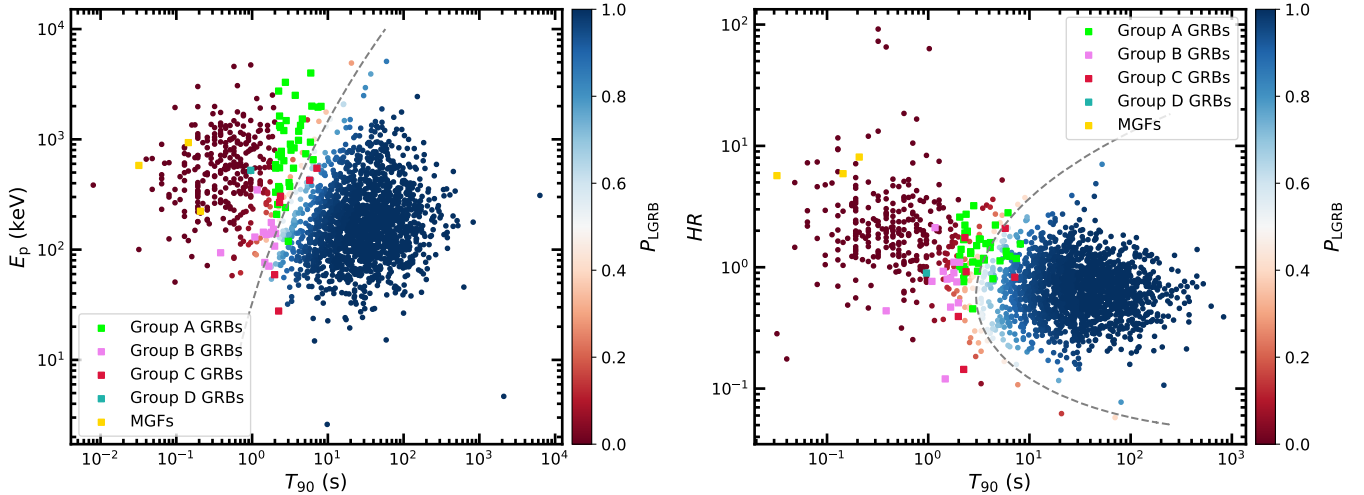


Figure 1. The E_p - T_{90} plane (left) and the HR - T_{90} plane (right). The colour of the data points from red to blue represents the probability of classification as LGRBs from 0 to 100%. The dashed line is the cutoff where the probability of LGRBs is 50%. The lime, violet, crimson, and lightseagreen squares represent the Group A, B, C, D GRBs, and MGFs, respectively.

$\varepsilon < 0.03$ and the rest frame duration $T_{90,z} < 5$ s. Subsequently, [Minaev & Pozanenko \(2020\)](#) found a boundary in the EH - T_{90} plane, and proposed a new parameter, the energy-hardness-duration $EHD = EH/T_{90,z}^{0.5}$, to classify GRBs with $EHD = 2.6$.

We calculated ε for peculiar GRBs at redshifts from 0.0001 to 10, as shown in Figure 3. Group A GRBs and Group B GRBs are significantly different from the trajectories of LGRBs and SGRBs in the ε - $T_{90,z}$ plane. In order to quantitatively study the classifications of peculiar GRBs, we obtain the redshift distribution of all GRBs with known redshifts and their cumulative distribution function (CDF), as shown in Figure 4. The redshifts of GRBs conform to a log-normal distribution with a median value of 1.31 and a dispersion of 0.41. Next, we calculate the redshift range (z_1 - z_2) of GRBs with $\varepsilon > 0.03$, where z_1 is the redshift corresponding to the $\varepsilon > 0.03$ for the first time as the redshift increases from 0.0001, and z_2 is the redshift corresponding to the $\varepsilon < 0.03$ for the first time as the redshift increases from z_1 to 10. Using the CDF, we then calculate the probability of redshift less than z_1 and z_2 , $P(z < z_1)$ and $P(z < z_2)$, respectively. The probability that the redshift of a GRB is within the redshift range making $\varepsilon > 0.03$ is $P_\varepsilon = P(z < z_2) - P(z < z_1)$, which are listed in Table 2. Note that, if ε is never larger than 0.03, then the $P_\varepsilon = 0$, and if ε is not less than 0.03 as the redshift increases from z_1 to 10, then $z_2 = 10$.

The values of ε of most Group A GRBs are less than 0.03 regardless of their redshift. Among them, GRB 090518080, GRB 100719825, GRB 150228845, GRB 161001045, and GRB 161210524 crossed the boundary in a very small redshift range, with a probability of less

than 50%, which indicates that they are classified as Type I GRBs. We calculated ε of GRB 161001045 and GRB 180618030, $\varepsilon = 0.014$ and $\varepsilon = 0.001$ respectively, which are classified as Type I GRBs. Group B GRBs are all classified as Type II GRBs within a redshift range of more than 60% probability. GRB 100816026 has $\varepsilon = 0.124$ and is classified as Type II GRB. For Group C GRBs, GRB 090320045 and GRB 101002279 with ε consistently less than 0.03 are classified as Type I GRBs. GRB 120504945 and GRB 140912664 with ε over 0.03 in the small redshift range are also classified as Type I GRBs. However, GRB 081130212 and GRB 131128629 with ε over 0.03 in the large redshift range are classified as Type II GRBs. Group D GRBs are classified as Type II GRBs in the redshift range with 73.8% probability.

We calculated the EH and EHD for peculiar GRBs at redshifts from 0.0001 to 10, as shown in Figure 5. We also calculated the redshift range of GRBs with $EHD < 2.6$ and calculate the probability that peculiar GRBs are within this redshift range using CDF, which is consistent with the method above. The results are listed in Table 2. Group A GRBs and Group B GRBs are significantly different from the trajectories of LGRBs and SGRBs in the EH - $T_{90,z}$ plane. Group A and D GRBs are all classified as Type I GRBs within a redshift range. GRB 161001045 and GRB 180618030 have $EHD = 3.46$ and $EHD = 13.98$, respectively, and are classified as Type I GRBs. Group B GRBs are classified as Type II GRBs except for GRB 140626843 which has a 39.3% probability in the redshift range of being classified as Type I GRBs. GRB 100816026 has $EHD = 1.17$ and is classified as Type II GRB. For Group C GRBs, GRB 090320045, GRB 101002279, GRB 120504945, and

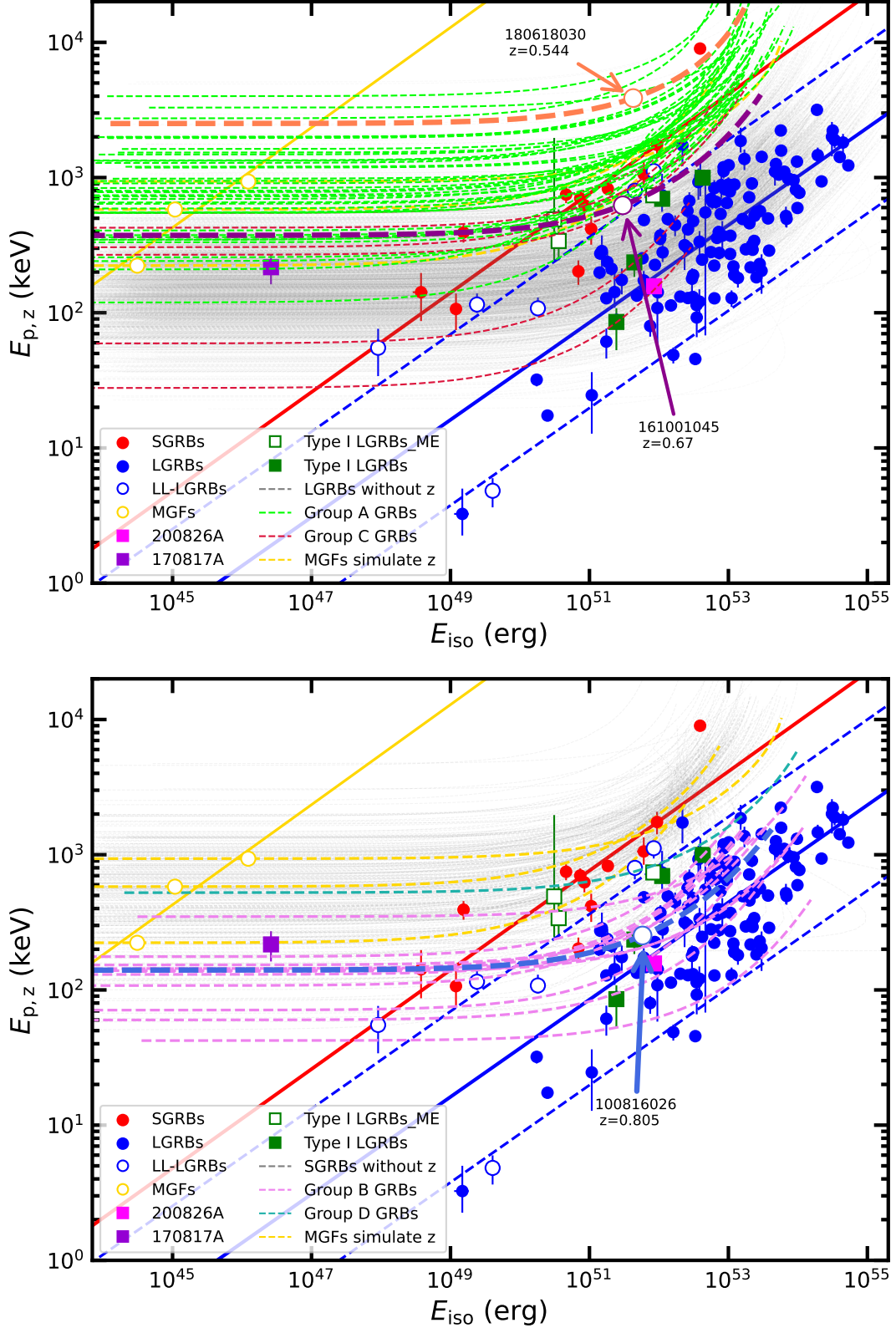


Figure 2. The $E_{p,z}$ - E_{iso} plane including the trajectories of Group A, C GRBs and LGRBs without z (top), and Group B, D GRBs and SGRBs without z (bottom). The red and blue solid lines are the best-fit lines for SGRBs and LGRBs fitted by the Markov Chain Monte Carlo (MCMC) method, respectively, and both are $E_{p,z} \propto E_{iso}^{0.37}$. The gold solid line is the translation of $E_{p,z} \propto E_{iso}^{0.37}$. The blue dashed lines are the 2σ confidence regions. The lime, violet, crimson, lightseagreen, gold, royalblue, darkmagenta, coral, and gray dashed lines are the trajectories that changes with redshift (gradually increasing from the left to the right) of Group A, B, C, D GRBs, MGFs, GRB 100816026, GRB 161001045, GRB 180618030, and LGRBs (SGRBs), respectively. The gold, royalblue, darkmagenta, coral, and gray rings are MGFs, GRB 100816026, GRB 161001045, and GRB 180618030 at their corresponding redshifts. The red points are SGRBs. The blue points and rings are LGRBs and low-luminosity LGRBs, respectively. The green squares and rings are Type I LGRBs and their MEs.

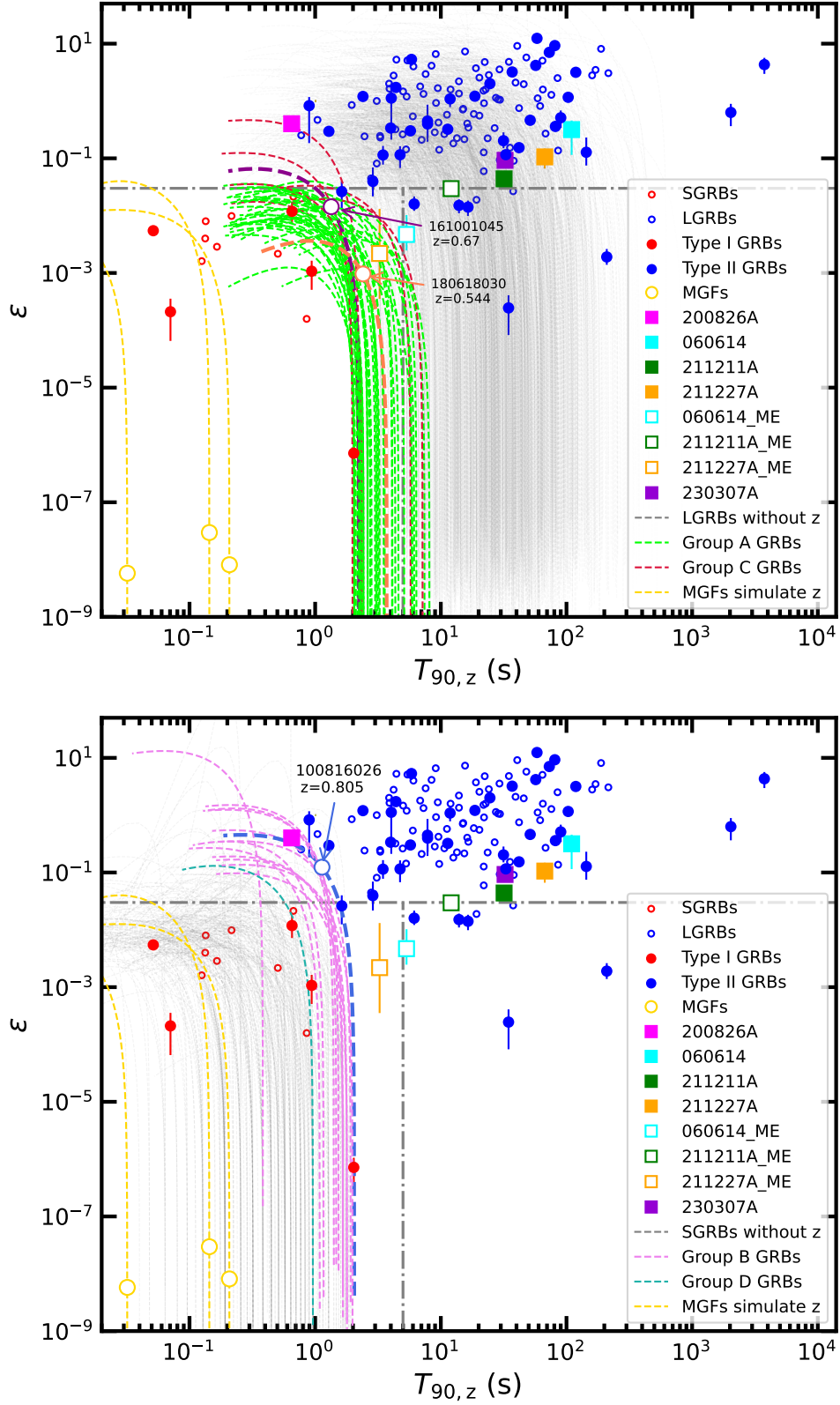


Figure 3. The ϵ - $T_{90,z}$ plane. The gray dotted lines are $\epsilon = 0.03$ and $T_{90,z} = 5$ s. The red rings and points are SGRBs and Type I GRBs. The blue rings and points are LGRBs and Type II GRBs. The redshift increases gradually from the bottom right to the top left.

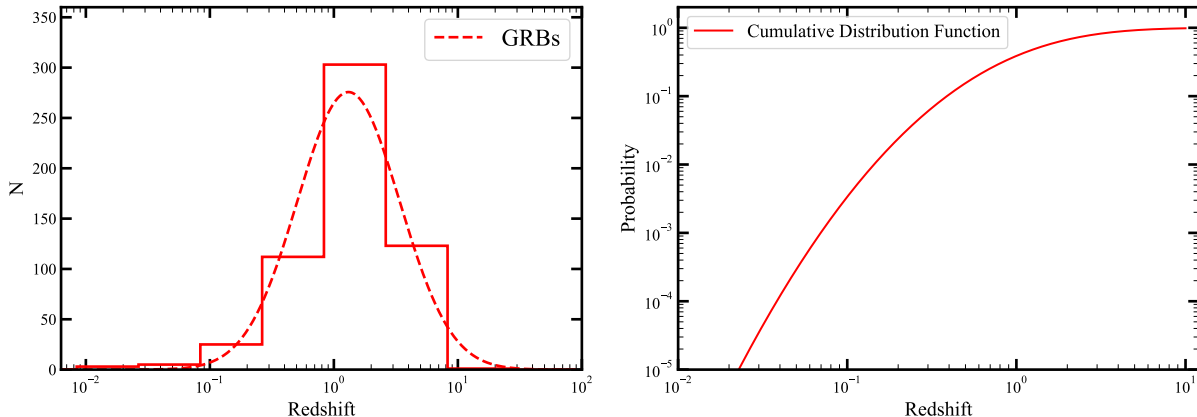


Figure 4. The redshift distributions of all GRBs with known redshift (left) and their cumulative distribution function (right). The red dotted line represents the best fitting with a lognormal function.

GRB 140912664 with EH consistently larger than 2.6 are classified as Type I GRBs. GRB 081130212 and GRB 131128629 have larger than 90% probability of being in the redshift range of being classified as Type II GRBs.

3.3. Spectral Lag

Spectral lag has been widely used to provide clues to the progenitors of GRBs. In addition, Norris et al. (2000) found that the isotropic luminosity–spectral lag ($L_{\text{iso}}-\tau$) correlation in the LGRBs, except for GRB 980425 that is a low-luminosity GRB and is associated with SN 1998bw. Ukwatta et al. (2012) further confirmed the $L_{\text{iso}}-\tau$ correlation by using τ extracted in the rest frame. However, Bernardini et al. (2015) raised concerns about the use of spectral lag to classify the progenitors of GRBs, as LGRBs do not always have significant spectral lag, which can significantly weaken the $L_{\text{iso}}-\tau$ correlation. They believed that the $L_{\text{iso}}-\tau$ correlation may only be a boundary. Li et al. (2023) found that Type I GRBs and Type II GRBs follow different $L_{\text{iso}}-\tau$ correlation, which may enable the identification of progenitors of GRBs. However, some Type II GRBs with high luminosity or negative spectral lag do not follow the $L_{\text{iso}}-\tau$ correlation of Type II GRBs. Although spectral lag can not provide conclusive evidence for identifying the progenitors of GRBs, it still provides key clues.

We use the cross-correlation function (CCF) to calculate the τ of lightcurves among different energy bands. For two lightcurves x_i and y_i , CCF is defined as (Band 1997)

$$\text{CCF}_{\text{Band}}(d, x, y) = \frac{\sum_{i=\max(1,1-d)}^{\min(N,N-d)} x_i y_{i+d}}{\sqrt{\sum_i x_i^2 \sum_i y_i^2}}, \quad (5)$$

where N is the total number of time bin (t_{bin}), d is the time delay in unit a t_{bin} . We fitted the CCF around

the peak with a polynomial to find d_{max} corresponding to its global maximum and calculated the spectral lag by $\tau = d \times t_{\text{bin}}$. The uncertainty of τ is estimated by Monte Carlo simulation (Ukwatta et al. 2010). In our analysis, we estimate the τ of 10–25 keV with respect to 50–100 keV (τ_{31}), the results are listed in Table 2.

The τ_{31} distributions and the $L_{\text{iso}}-\tau_{31,z}$ plane are shown in Figure 6 and Figure 7, respectively, where $\tau_{31,z} = \tau_{31}/(1+z)$. We find no significant difference in the distribution of τ between different groups nor between them and Type I GRBs and Type II GRBs. However, 14 Group A GRBs, accounting for about 34%, have negative τ , which suggests that they are more likely to be SGRBs than LGRBs. When only GRBs with positive $\tau_{31,z}$ are considered, there is a weak correlation $L_{\text{iso}} \propto \tau_{31,z}^{-2.45}$ between L_{iso} and $\tau_{31,z}$ of both Type I GRBs and SGRBs, with a Pearson's coefficient $r = -0.75$, whereas Type II GRBs are not. Although the $L_{\text{iso}}-\tau_{31,z}$ correlation does not exist in Type II GRBs, it seems to serve as a dividing line to classify the different progenitors of GRBs. If, as we expect, Group A GRBs have smaller redshifts and Group B GRBs have larger redshifts, this will support the notion that mergers are origin of Group A GRBs and collapsars are origin of Group B GRBs. However, counter examples do exist - $\tau = 150 \pm 15$ ms of GRB 170817A is significantly larger than that of GRB 200826A, and τ of GRB 180728A is even negative. This suggests that using τ alone as the only indicator cannot reliably differentiate progenitors.

4. DISCUSSION

All Group A GRBs are classified as Type I GRBs in both the $\varepsilon-T_{90,z}$ and the $EH-T_{90,z}$ planes. 10 Group A GRBs are classified as LGRBs in the E_p-T_{90} plane or the $HR-T_{90}$ plane, and only GRB 081006604 is classified as LGRBs at the same time. GRB 161001045 and GRB 180618030 have $z = 0.67$ and $z = 0.554$, respectively,

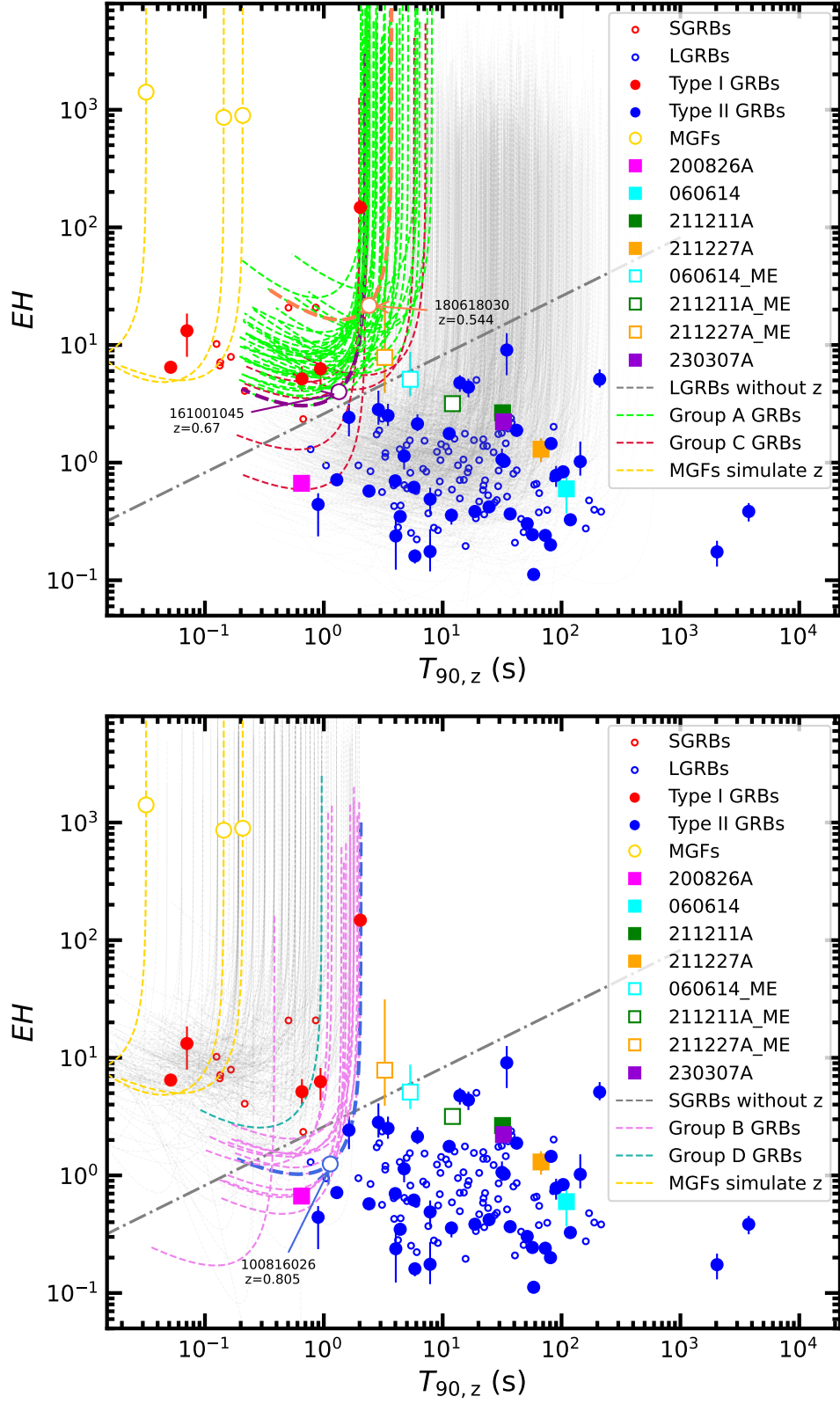


Figure 5. The $EH-T_{90,z}$ plane. The gray dotted line is $EHD = 2.6$. The redshift increases gradually from the top right to the bottom left.

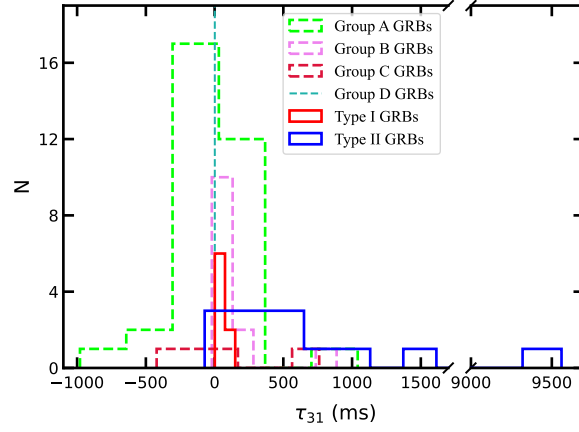


Figure 6. The τ_{31} distributions of Group A, B, C, and D GRBs, Type I GRBs and Type II GRBs.

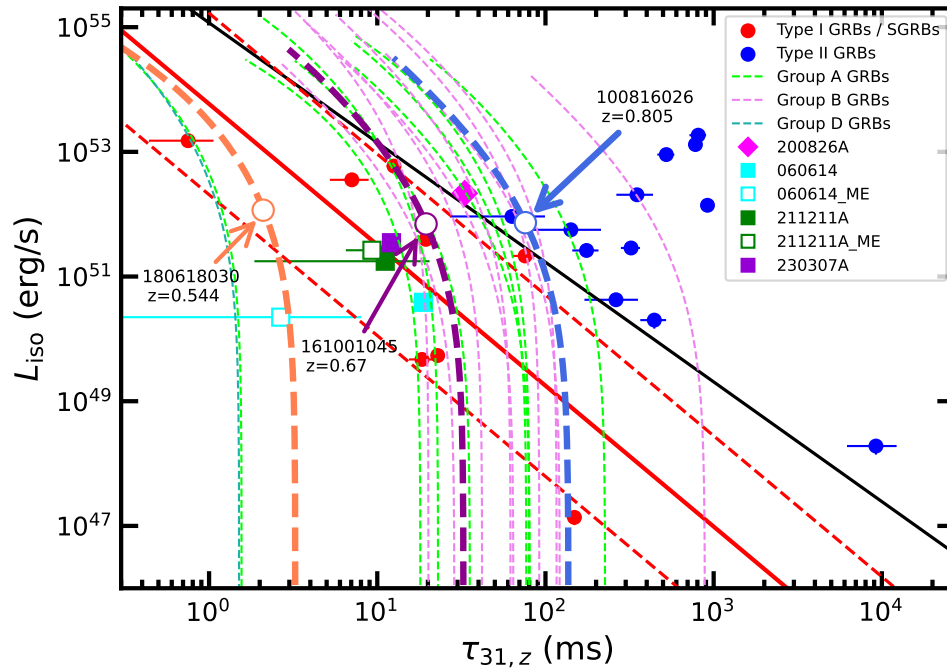


Figure 7. The $L_{\text{iso}} - \tau_{31,z}$ plane. The black solid line is the possible dividing line. The red solid line is the best-fit line for Type I GRBs/SGRBs. The red dashed lines are the confidence regions of 2σ . The redshift increases gradually from the bottom right to the top left.

and are classified as Type I GRBs in both the $\varepsilon-T_{90,z}$ and the $EH-T_{90,z}$ planes. Moreover, according to the two type progenitors of GRBs, the properties of their host galaxies and GRB offset from the host galaxy center are significantly different (Zhang et al. 2009; Fong et al. 2010; Li et al. 2016, 2020; Fong et al. 2022; Nugent et al. 2022). GRBs originating from mergers are usually located in the dwarf and elliptical galaxies, and have larger offset from the galactic center, their host galaxies also have smaller star formation rate (SFR) and smaller specific star formation rate (sSFR, $sSFR = SFR/M_\odot$, where M_\odot is the stellar mass of the host galaxy), since the SN that needs to be experienced in the formation of an NS or BH kicks the progenitor away from the star-forming region of the host galaxy to bring about a larger offset (Berger et al. 2005; Gehrels et al. 2005; Fong et al. 2022; Nugent et al. 2022). However, GRBs originating from collapsars are usually located in the bright regions of the irregular and dwarf galaxies, where they exhibit a small offset and a large star formation rate. GRB 161001045 is 18.54 ± 6.22 kpc away from the host galaxy, which is consistent with the merger origin (Fong et al. 2022). Meanwhile, the host galaxy of GRB 161001045 with $SFR = 0.53_{-0.31}^{+0.59} M_\odot \text{ yr}^{-1}$ and $\log(sSFR) = -10.02_{-0.37}^{+0.33} \text{ yr}^{-1}$ is a low-SFR galaxy. This is also consistent with the merger origin (Nugent et al. 2022). GRB 180618030 has an offset 9.7 ± 1.69 kpc from the host galaxy with an $SFR = 1.85_{-1.10}^{+1.77} M_\odot \text{ yr}^{-1}$ and $\log(sSFR) = -8.54_{-0.39}^{+0.44} \text{ yr}^{-1}$, which is consistent with the merger origin (Fong et al. 2022; Nugent et al. 2022). In total, 17 Group A GRBs are suggested by all 5 indicators, including τ , to be originated by mergers.

Among Group B GRBs, only GRB 140626843 is classified as Type I GRB in the $EH-T_{90,z}$ plane, and all other GRBs are classified as Type II GRBs in both the $\varepsilon-T_{90,z}$ and the $EH-T_{90,z}$ planes. However, the extremely large τ of GRB 140626843 strongly supports its collapsar origin. Despite the fact that classifications in both the E_p-T_{90} and the $HR-T_{90}$ planes do not support their collapsar origins while considering that GRB 200826A would be equally unsupported as a collapsar origin, we nevertheless argue that they should be collapsar origins.

Among Group C GRBs, GRB 081130212 and GRB 131128629 are classified as Type II GRBs, and other GRBs are classified as Type I GRBs in both the $\varepsilon-T_{90,z}$ and the $EH-T_{90,z}$ planes. GRB 090320045 and GRB 140912664 are classified as Type I GRBs and other GRBs are classified as Type II GRBs in the E_p-T_{90} plane. GRB 101002279 and GRB 12050494 are classified as Type II GRBs and other GRBs are classified as Type I GRBs in the $HR-T_{90}$ plane. Just merger origins

of GRB 090320045 and GRB 140912664 are supported by 4 clues.

Among Group D GRBs, GRB 150819440 is classified as Type II GRB in the $\varepsilon-T_{90,z}$ plane and is classified as Type I GRB in the other planes, therefore we can not determine its origin.

We compared the trajectories of MGFs with SGRBs in the $E_{p,z}-E_{\text{iso}}$, the $\varepsilon-T_{90,z}$, the $EH-T_{90,z}$ planes and found that they are not significantly different from SGRBs, and thus only precise localization is possible for identification. Since all known durations of MGFs are significantly smaller than those of GRBs in our sample, they are not considered as being MGFs in this work.

5. CONCLUSIONS

The identification of progenitors of GRBs is crucial for studying the physical mechanisms of GRBs. Currently, convincing evidence to a certain type of progenitors comes from optical afterglow, with KNe pointing to mergers and SNe to collapsars. However, KN/SN is dependent on high-precision multiband observations, which are bound to be lacking for the vast majority of GRBs. The prompt emissions of GRBs also provide key clues to identify their progenitors, such as T_{90} , E_p , and τ , especially when their redshift can be detected. T_{90} has been used as an excellent alternative because it can be extracted in the lightcurves of almost all GRBs. The earlier observed KNe/SNe corresponds perfectly with the T_{90} classification. However, GRB 200826A and GRB 211211A break the correspondence between the progenitors and T_{90} .

In this work, we attempted to determine the progenitors of peculiar GRBs that are identified through machine learning. The peculiar GRBs are divided into four groups, depending on the machine learning classification results. In order to verify whether long GRBs-I and short GRBs-II originated from mergers and collapsars, respectively, we investigated them from the E_p-T_{90} , the $HR-T_{90}$, the $E_{p,z}-E_{\text{iso}}$, the $\varepsilon-T_{90,z}$, the $EH-T_{90,z}$, and the $L_{\text{iso}}-\tau_{31,z}$ planes.

Finally, we found 17 long Type I GRB candidates and 13 short Type II GRB candidates, greatly expanding the sample of peculiar GRBs. As a result of the analysis above, our conclusions are as follows:

1. There are 17 Group A GRBs, including GRB 161001045 and GRB 180618030, which are LGRBs but their τ are smaller than typical LGRBs. Meanwhile, they have a less than 50% probability of being classified as LGRBs in both the E_p-T_{90} and the $HR-T_{90}$ planes. Moreover, in the $E_{p,z}-E_{\text{iso}}$, the $\varepsilon-T_{90,z}$, and the $EH-T_{90,z}$ planes, they demonstrate distinct properties compared to

LGRBs and Type II GRBs. The host galaxy characteristics of both GRB 161001045 and GRB 180618030 are also consistent with a merger scenario. Although their T_{90} are shorter than WE durations of long Type I GRBs, they are similar to ME durations of long Type I GRBs. These are strong evidence supporting their merger origin. Unfortunately, multiwavelength observations are lacking. Assuming that Group A GRBs are indeed originated from mergers, this suggests that the population of long Type I GRBs is not scarce and that the lack of high-precision observations has prevented us from identifying them. Meanwhile, the timescale of compact binary mergers can extend to the same timescales of MEs of long Type I GRBs, which implies that EEs of long Type I GRBs may involve a distinct physical mechanism compared to MEs.

2. Similar to GRB 200826A, GRB 100816026 has a τ larger than typical SGRBs and is consistent with LGRBs and Type II GRBs in the $E_{p,z}-E_{\text{iso}}$, $\varepsilon-T_{90,z}$ and the $EH-T_{90,z}$ planes, so it should originate from a collapsar. Although the absence of redshift does not allow the other Group B GRBs to be unambiguously localized in the $E_{p,z}-E_{\text{iso}}$, the $\varepsilon-T_{90,z}$, and the $EH-T_{90,z}$ planes, the proba-

bility of them belonging to Type II GRBs given by the distribution of redshifts strongly supports their collapsar origin. Assuming that Group B GRBs indeed originated from collapsars, this suggests that the population of long Type II GRBs is not scarce, which is unfavourable to the interpretation that the jet progression leading to a missed ME.

3. The origins of Group C GRBs are mixed, GRB 081130212 and GRB 131128629 are likely to have collapsar origin but GRB 090320045, GRB 101002279, and GRB 140912664 are likely to have merger origin.
4. GRB 150819440 is classified as Type II GRB in the $\varepsilon-T_{90,z}$ plane and is classified as Type I GRBs in the other planes. The origin of Group D is also ambiguous.

ACKNOWLEDGMENTS

We thank the anonymous reviewers for their insightful comments/suggestions. We acknowledge the use of public data and software provided by the Fermi Science Support Center. This work was supported in part by the National Natural Science Foundation of China (No. 12273122).

REFERENCES

- Abbott, B. P., Abbott, R., Abbott, T. D., et al. 2017, *ApJL*, 848, L13. doi:10.3847/2041-8213/aa920c
- Abbott, B. P., Abbott, R., Abbott, T. D., et al. 2017, *PhRvL*, 119, 161101. doi:10.1103/PhysRevLett.119.161101
- Ahumada, T., Singer, L. P., Anand, S., et al. 2021, *Nature Astronomy*, 5, 917. doi:10.1038/s41550-021-01428-7
- Aloy, M. A., Janka, H.-T., & Müller, E. 2005, *A&A*, 436, 273. doi:10.1051/0004-6361:20041865
- Amati, L., Frontera, F., Tavani, M., et al. 2002, *A&A*, 390, 81. doi:10.1051/0004-6361:20020722
- Amati, L. 2006, *MNRAS*, 372, 233. doi:10.1111/j.1365-2966.2006.10840.x
- Amati, L. 2021, *Nature Astronomy*, 5, 877. doi:10.1038/s41550-021-01401-4
- Band, D., Matteson, J., Ford, L., et al. 1993, *ApJ*, 413, 281. doi:10.1086/172995
- Band, D. L. 1997, *ApJ*, 486, 928. doi:10.1086/304566
- Barnes, J. & Metzger, B. D. 2023, *ApJ*, 947, 55. doi:10.3847/1538-4357/acc384
- Berger, E., Price, P. A., Cenko, S. B., et al. 2005, *Nature*, 438, 988. doi:10.1038/nature04238
- Bernardini, M. G., Ghirlanda, G., Campana, S., et al. 2015, *MNRAS*, 446, 1129. doi:10.1093/mnras/stu2153
- Bhardwaj, S., Dainotti, M. G., Venkatesh, S., et al. 2023, *MNRAS*, 525, 5204. doi:10.1093/mnras/stad2593
- Bissaldi, E., McBreen, S., & Connaughton, V. 2008, GRB Coordinates Network, Circular Service, No. 8369, #1 (2008), 8369
- Chen, J.-M., Zhu, K.-R., Peng, Z.-Y., et al. 2024, *MNRAS*, 527, 4272. doi:10.1093/mnras/stad3407
- Cheng, L. X., Ma, Y. Q., Cheng, K. S., et al. 1995, *A&A*, 300, 746
- Della Valle, M., Chincarini, G., Panagia, N., et al. 2006, *Nature*, 444, 1050. doi:10.1038/nature05374
- Dimple, Misra, K., & Arun, K. G. 2023, *ApJL*, 949, L22. doi:10.3847/2041-8213/acd4c4
- Fan, Y.-Z. & Wei, D.-M. 2011, *ApJ*, 739, 47. doi:10.1088/0004-637X/739/1/47
- Fong, W., Berger, E., & Fox, D. B. 2010, *ApJ*, 708, 9. doi:10.1088/0004-637X/708/1/9
- Fong, W.-. fai ., Nugent, A. E., Dong, Y., et al. 2022, *ApJ*, 940, 56. doi:10.3847/1538-4357/ac91d0

- Fynbo, J. P. U., Watson, D., Thöne, C. C., et al. 2006, *Nature*, 444, 1047. doi:10.1038/nature05375
- Gal-Yam, A., Fox, D. B., Price, P. A., et al. 2006, *Nature*, 444, 1053. doi:10.1038/nature05373
- Gao, H., Zhang, B., Lü, H.-J., et al. 2017, *ApJ*, 837, 50. doi:10.3847/1538-4357/aa5be3
- Gehrels, N., Sarazin, C. L., O'Brien, P. T., et al. 2005, *Nature*, 437, 851. doi:10.1038/nature04142
- Gehrels, N., Norris, J. P., Barthelmy, S. D., et al. 2006, *Nature*, 444, 1044. doi:10.1038/nature05376
- Goldstein, A., Preece, R. D., Mallozzi, R. S., et al. 2013, *ApJS*, 208, 21. doi:10.1088/0067-0049/208/2/21
- Golenetskii, S., Aptekar, R., Mazets, E., et al. 2011, GRB Coordinates Network, Circular Service, No. 12663, #1 (2011), 12663
- Gruber, D., Goldstein, A., Weller von Ahlefeld, V., et al. 2014, *ApJS*, 211, 12. doi:10.1088/0067-0049/211/1/12
- Jespersen, C. K., Severin, J. B., Steinhardt, C. L., et al. 2020, *ApJL*, 896, L20. doi:10.3847/2041-8213/ab964d
- Jin, Z.-P., Hotokezaka, K., Li, X., et al. 2016, *Nature Communications*, 7, 12898. doi:10.1038/ncomms12898
- Jordana-Mitjans, N., Mundell, C. G., Guidorzi, C., et al. 2022, *ApJ*, 939, 106. doi:10.3847/1538-4357/ac972b
- Kaneko, Y., Ramirez-Ruiz, E., Granot, J., et al. 2007, *ApJ*, 654, 385. doi:10.1086/508324
- King, A., Olsson, E., & Davies, M. B. 2007, *MNRAS*, 374, L34. doi:10.1111/j.1745-3933.2006.00259.x
- Kouveliotou, C., Meegan, C. A., Fishman, G. J., et al. 1993, *ApJL*, 413, L101. doi:10.1086/186969
- Levan, A. J., Gompertz, B. P., Salafia, O. S., et al. 2024, *Nature*, 626, 737. doi:10.1038/s41586-023-06759-1
- Li, Y., Zhang, B., & Lü, H.-J. 2016, *ApJS*, 227, 7. doi:10.3847/0067-0049/227/1/7
- Li, Y., Zhang, B., & Yuan, Q. 2020, *ApJ*, 897, 154. doi:10.3847/1538-4357/ab96b8
- Li, Q. M., Zhang, Z. B., Han, X. L., et al. 2023, *MNRAS*, 524, 1096. doi:10.1093/mnras/stad1648
- Lien, A., Sakamoto, T., Barthelmy, S. D., et al. 2016, *ApJ*, 829, 7. doi:10.3847/0004-637X/829/1/7
- Lü, H.-J., Liang, E.-W., Zhang, B.-B., et al. 2010, *ApJ*, 725, 1965. doi:10.1088/0004-637X/725/2/1965
- Laurens van der Maaten. & Geoffrey Hinton. 2008, *Journal of Machine Learning Research*, 9, 2579.
- Laurens van der Maaten. 2014, *Journal of Machine Learning Research*, 15, 3321.
- MacFadyen, A. I. & Woosley, S. E. 1999, *ApJ*, 524, 262. doi:10.1086/307790
- McInnes, L., Healy, J., & Melville, J. 2018, arXiv:1802.03426
- Meegan, C., Lichti, G., Bhat, P. N., et al. 2009, *ApJ*, 702, 791. doi:10.1088/0004-637X/702/1/791
- Mereghetti, S., Rigoselli, M., Salvaterra, R., et al. 2024, *Nature*, 629, 58. doi:10.1038/s41586-024-07285-4
- Minaev, P. Y. & Pozanenko, A. S. 2020, *MNRAS*, 492, 1919. doi:10.1093/mnras/stz3611
- Nicuesa Guelbenzu, A., Kloze, S., Rossi, A., et al. 2011, *A&A*, 531, L6. doi:10.1051/0004-6361/201116657
- Norris, J. P., Share, G. H., Messina, D. C., et al. 1986, *ApJ*, 301, 213. doi:10.1086/163889
- Norris, J. P., Marani, G. F., & Bonnell, J. T. 2000, *ApJ*, 534, 248. doi:10.1086/308725
- Nugent, A. E., Fong, W.-F., Dong, Y., et al. 2022, *ApJ*, 940, 57. doi:10.3847/1538-4357/ac91d1
- Ofek, E. O., Kulkarni, S. R., Nakar, E., et al. 2006, *ApJ*, 652, 507. doi:10.1086/507837
- Ofek, E. O., Munro, M., Quimby, R., et al. 2008, *ApJ*, 681, 1464. doi:10.1086/587686
- Paczynski, B. 1986, *ApJL*, 308, L43. doi:10.1086/184740
- Qin, Y.-P. & Chen, Z.-F. 2013, *MNRAS*, 430, 163. doi:10.1093/mnras/sts547
- Rastinejad, J. C., Gompertz, B. P., Levan, A. J., et al. 2022, *Nature*, 612, 223. doi:10.1038/s41586-022-05390-w
- Roberts, O. J., Veres, P., Baring, M. G., et al. 2021, *Nature*, 589, 207. doi:10.1038/s41586-020-03077-8
- Roberts, O. J., Meegan, C., Lesage, S., et al. 2023, GRB Coordinates Network, Circular Service, No. 34391, 34391
- Rossi, A., Rothberg, B., Palazzi, E., et al. 2022, *ApJ*, 932, 1. doi:10.3847/1538-4357/ac60a2
- Sakamoto, T., Lamb, D. Q., Graziani, C., et al. 2004, *ApJ*, 602, 875. doi:10.1086/381232
- Schaefer, B. E. 2007, *ApJ*, 660, 16. doi:10.1086/511742
- Stamatikos, M., Barthelmy, S. D., Baumgartner, W. H., et al. 2013, GRB Coordinates Network, Circular Service, No. 15316, #1 (2013), 15316
- Stanek, K. Z., Matheson, T., Garnavich, P. M., et al. 2003, *ApJL*, 591, L17. doi:10.1086/376976
- Steinhardt, C. L., Mann, W. J., Rusakov, V., et al. 2023, *ApJ*, 945, 67. doi:10.3847/1538-4357/acb999
- Svinkin, D., Golenetskii, S., Aptekar, R., et al. 2018, GRB Coordinates Network, Circular Service, No. 23495, #1 (2018/December-0), 23495
- Svinkin, D., Frederiks, D., Hurley, K., et al. 2021, *Nature*, 589, 211. doi:10.1038/s41586-020-03076-9
- Trigg, A. C., Burns, E., Roberts, O. J., et al. 2024, *A&A*, 687, A173. doi:10.1051/0004-6361/202348858
- Troja, E., Fryer, C. L., O'Connor, B., et al. 2022, *Nature*, 612, 228. doi:10.1038/s41586-022-05327-3
- Tsutsui, R. & Shigeyama, T. 2014, *PASJ*, 66, 42. doi:10.1093/pasj/psu008

- Tsvetkova, A., Frederiks, D., Golenetskii, S., et al. 2017a, *ApJ*, 850, 161. doi:10.3847/1538-4357/aa96af
- Tsvetkova, A., Frederiks, D., Svinkin, D., et al. 2021, *ApJ*, 908, 83. doi:10.3847/1538-4357/abd569
- Tsvetkova, A., Frederiks, D., Lysenko, A., et al. 2022, GRB Coordinates Network, Circular Service, No. 31544, 31544
- Ukwatta, T. N., Stamatikos, M., Dhuga, K. S., et al. 2010, *ApJ*, 711, 1073. doi:10.1088/0004-637X/711/2/1073
- Ukwatta, T. N., Dhuga, K. S., Stamatikos, M., et al. 2012, *MNRAS*, 419, 614. doi:10.1111/j.1365-2966.2011.19723.x
- von Kienlin, A., Meegan, C. A., Paciesas, W. S., et al. 2020, *ApJ*, 893, 46. doi:10.3847/1538-4357/ab7a18
- Wang, H., Zhang, F.-W., Wang, Y.-Z., et al. 2017, *ApJL*, 851, L18. doi:10.3847/2041-8213/aa9e08
- Wang, X. I., Zhang, B.-B., & Lei, W.-H. 2022, *ApJL*, 931, L2. doi:10.3847/2041-8213/ac6c7e
- Wiersema, K., van der Horst, A. J., Kann, D. A., et al. 2008, *A&A*, 481, 319. doi:10.1051/0004-6361:20078050
- Woosley, S. E. 1993, *ApJ*, 405, 273. doi:10.1086/172359
- Xin, L.-P., Liang, E.-W., Wei, J.-Y., et al. 2011, *MNRAS*, 410, 27. doi:10.1111/j.1365-2966.2010.17419.x
- Yamazaki, R., Yonetoku, D., & Nakamura, T. 2003, *ApJL*, 594, L79. doi:10.1086/378736
- Yang, B., Jin, Z.-P., Li, X., et al. 2015, *Nature Communications*, 6, 7323. doi:10.1038/ncomms8323
- Yang, J., Chand, V., Zhang, B.-B., et al. 2020, *ApJ*, 899, 106. doi:10.3847/1538-4357/aba745
- Yang, J., Ai, S., Zhang, B.-B., et al. 2022, *Nature*, 612, 232. doi:10.1038/s41586-022-05403-8
- Yang, Y.-H., Troja, E., O'Connor, B., et al. 2024, *Nature*, 626, 742. doi:10.1038/s41586-023-06979-5
- Yi, T., Liang, E., Qin, Y., et al. 2006, *MNRAS*, 367, 1751. doi:10.1111/j.1365-2966.2006.10083.x
- Yin, Y.-H. I., Zhang, Z. J., Yang, J., et al. 2024, *ApJL*, 963, L10. doi:10.3847/2041-8213/ad2839
- Zhang, B., Zhang, B.-B., Liang, E.-W., et al. 2007, *ApJL*, 655, L25. doi:10.1086/511781
- Zhang, B., Zhang, B.-B., Virgili, F. J., et al. 2009, *ApJ*, 703, 1696. doi:10.1088/0004-637X/703/2/1696
- Zhang, F.-W., Shao, L., Yan, J.-Z., et al. 2012, *ApJ*, 750, 88. doi:10.1088/0004-637X/750/2/88
- Zhang, Z.-B., Yang, E.-B., Choi, C.-S., et al. 2016, *MNRAS*, 462, 3243. doi:10.1093/mnras/stw1835
- Zhang, Z. B., Zhang, C. T., Zhao, Y. X., et al. 2018, *PASP*, 130, 054202. doi:10.1088/1538-3873/aaa6af
- Zhang, H.-M., Liu, R.-Y., Zhong, S.-Q., et al. 2020, *ApJL*, 903, L32. doi:10.3847/2041-8213/abc2c9
- Zhang, B.-B., Liu, Z.-K., Peng, Z.-K., et al. 2021, *Nature Astronomy*, 5, 911. doi:10.1038/s41550-021-01395-z
- Zhong, S.-Q., Li, L., & Dai, Z.-G. 2023, *ApJL*, 947, L21. doi:10.3847/2041-8213/acca83
- Zhu, J.-P., Wang, X. I., Sun, H., et al. 2022, *ApJL*, 936, L10. doi:10.3847/2041-8213/ac85ad
- Zhu, S.-Y., Liu, Z.-Y., Shi, Y.-R., et al. 2023, *ApJ*, 950, 30. doi:10.3847/1538-4357/acc83b
- Zhu, S.-Y., Sun, W.-P., Ma, D.-L., et al. 2024, *MNRAS*, 532, 1434. doi:10.1093/mnras/stae1594

Table 1. The prompt emission parameters of GRBs associated with SN or GW/KN observations in the sample

<i>GRB</i>	<i>z</i>	<i>T</i> ₉₀ (s)	<i>τ</i> ₃₁ (ms)	<i>model</i>	<i>E_p</i> (keV)	<i>α</i>	<i>β</i>	<i>S</i> _{γ-6} (erg cm ⁻²)	<i>F</i> _{p-6} (erg cm ⁻² s ⁻¹)	<i>E</i> _{range}	<i>E</i> _{iso,50} (erg)	<i>L</i> _{iso,50} (erg s ⁻¹)	<i>Ass.</i>	<i>Ref.</i>
970228	0.695	53.44 ± 2.89	-	CPL	165 ⁺³⁹ ₋₂₅	-1.27	-	8.07 ± 0.49	4.59 ± 0.8	10-10000	113 ^{+6.84} _{-6.84}	109 ^{+18.9} _{-18.9}	SN	(1)
980326	0.9	9 ± 0.9	-	Band	92 ⁺²⁰ ₋₂₀	-1.23	-2.48	0.76 ± 0.15	0.25 ± 0.02	40-700	29.2 ^{+5.77} _{-5.77}	17.9 ^{+1.1} _{-1.1}	SN	(2)
980425	0.0085	34.88 ± 3.78	-	Band	54.6 ^{+20.9} _{-20.9}	-1	-2.1	4 ± 0.74	0.29 ± 0.02	20-2000	0.0091 ^{+0.0017} _{-0.0017}	0.0007 ^{+0.0004} _{-0.0004}	SN	(3),(4)
990712	0.434	20 ± 2	-	Band	779 ⁺¹²⁵ ₋₁₂₅	-1.88	-2.48	6.5 ± 0.3	1.3 ± 0.1	40-700	84.2 ^{+3.89} _{-3.89}	24.1 ^{+1.86} _{-1.86}	SN	(2)
991208	0.706	63.06 ± 0.48	-	Band	185 ⁺⁵ ₋₅	-1.27	-2.92	155 ± 2.9	22 ± 1.1	10-10000	2180 ^{+40.7} _{-40.7}	527 ^{+26.4} _{-26.4}	SN	(1)
000911	1.058	23.35 ± 0.23	-	Band	1083 ⁺⁵² ₋₅₂	-0.82	-2.75	208 ± 6.5	29 ± 2.8	10-10000	5680 ⁺¹⁷⁷ ₋₁₇₇	1630 ⁺¹⁵⁷ ₋₁₅₇	SN	(1)
011121	0.36	57.01 ± 3.78	-	Band	819 ⁺¹⁰⁸ ₋₁₀₈	-1.26	-2.01	279 ± 7.5	28.2 ± 2.3	10-10000	852 ^{+22.9} _{-22.9}	117 ^{+9.56} _{-9.56}	SN	(1)
020405	0.69	41.54 ± 2.03	-	Band	161 ⁺⁷ ₋₇	-0.97	-2.6	83.7 ± 1.2	8.16 ± 0.93	10-10000	1060 ^{+15.3} _{-15.3}	175 ⁺²⁰ ₋₂₀	SN	(1)
020903	0.251	9.8 ± 0.6	-	CPL	2.6 ^{+1.4} _{-0.8}	-1	-	0.06 ± 0.01	0.01 ± 0.01	2-10	0.15 ^{+0.04} _{-0.04}	0.05 ± 0.02	-	(5)
021211	1.01	1.8 ± 0.25	-	CPL	54 ⁺²⁵ ₋₂₅	-1.43	-	2.62 ± 0.26	2.62 ± 0.4	10-10000	95 ^{+9.43} _{-9.43}	191 ^{+29.2} _{-29.2}	SN	(1)
030329	0.168	21.81 ± 1.15	-	Band	97 ⁺² ₋₂	-1.53	-2.78	187 ± 2.6	24.7 ± 1.4	10-10000	149 ^{+2.07} _{-2.07}	23 ^{+1.3} _{-1.3}	SN	(1)
040924	0.859	2.39 ± 0.24	-	CPL	72 ⁺⁶ ₋₆	-0.55	-	2.31 ± 0.07	3.99 ± 0.5	10-10000	48.1 ^{+1.35} _{-1.35}	154 ^{+19.3} _{-19.3}	SN	(1),(6)
041006	0.716	6.85 ± 1.98	-	CPL	86 ⁺⁵ ₋₅	0.08	-	4.72 ± 0.25	2.27 ± 0.48	10-10000	64.5 ^{+3.42} _{-3.42}	53.3 ^{+11.3} _{-11.3}	SN	(1)
050416A	0.6535	6.67 ± 3.42	-	CPL	14.85 ^{+7.13} _{-7.13}	-0.82	-	0.37 ± 0.05	0.19 ± 0.02	15-150	10.8 ^{+1.46} _{-1.46}	9.12 ^{+0.9} _{-0.9}	-	(7)
050525A	0.606	7.05 ± 0.19	562.01 ± 138.09	Band	80 ⁺² ₋₂	-1.05	-3.2	24.6 ± 0.44	12 ± 0.73	10-10000	262 ^{+4.68} _{-4.68}	205 ^{+12.5} _{-12.5}	-	(1),(8)
060218	0.0331	2100 ± 100	-	Band	4.67 ^{+1.12} _{-1.12}	-1.44	-2.54	17.2 ± 1.8	0.0011 ± 0.0005	0.5-150	0.4 ^{+0.04} _{-0.04}	0.00003 ^{+0.00001} _{-0.00001}	-	(9)
060614	0.125	123.65 ± 18.94	21.2 ± 2.86	CPL	76 ⁺²⁰ ₋₂₀	-1.92	-	47 ± 2.6	6.6 ± 1.3	10-10000	24.4 ^{+1.35} _{-1.35}	3.86 ^{+0.76} _{-0.76}	KN	(10)
060614*	0.125	6 ± 0.6	3 ± 6	CPL	302 ⁺²¹⁴ ₋₈₅	-1.57	-	8.19 ± 0.56	4.5 ± 0.72	20-20000	3.6 ^{+0.25} _{-0.25}	2.23 ^{+0.36} _{-0.36}	KN	(10),(11)
070714B	0.92	1.26 ± 0.17	24.14 ± 2.31	CPL	551 ⁺¹⁴⁸ ₋₁₁₂	0.19	-	2.71 ± 0.54	13.8 ± 3.1	10-10000	60.5 ^{+12.1} _{-12.1}	591 ⁺¹³³ ₋₁₃₃	KN	(1)
071112C	0.823	5.25 ± 0.83	-	CPL	406 ⁺¹⁰⁰ ₋₁₀₀	-1.13	-	6.02 ± 1.11	3.8 ± 1.1	10-10000	111 ^{+20.5} _{-20.5}	128 ⁺³⁷ ₋₃₇	SN	(1)
080319B	1.95	10.23 ± 0.64	2298.46 ± 59.46	CPL	632 ⁺¹⁶⁰ ₋₁₁₃	-1.21	-	15.5 ± 1.8	4.61 ± 0.83	10-10000	1500 ⁺¹⁷⁴ ₋₁₇₄	1310 ⁺²³⁷ ₋₂₃₇	SN	(1)
080905	0.1218	0.96 ± 0.35	-	CPL	349.71 ^{+55.27} _{-55.27}	0.2	-	0.45 ± 0.06	1.97 ± 0.21	10-10000	0.15 ^{+0.02} _{-0.02}	0.76 ^{+0.08} _{-0.08}	-	(12)
080905B	2.374	105.98 ± 6.8	-	CPL	199.14 ^{+31.41} _{-31.41}	-0.88	-	1.96 ± 0.22	0.53 ± 0.14	10-10000	274 ^{+30.7} _{-30.7}	249 ^{+67.1} _{-67.1}	-	(12)
080916	0.689	46.34 ± 7.17	-	Band	105.73 ^{+20.45} _{-20.45}	-0.78	-1.77	12.8 ± 0.4	1.05 ± 0.2	10-10000	299 ^{+9.22} _{-9.22}	41.3 ^{+7.87} _{-7.87}	-	(12)
081007	0.5295	12 ± 0.12	401.73 ± 140.92	CPL	40 ⁺¹⁰ ₋₁₀	-1.4	-	1.2 ± 0.1	0.19 ± 0.02	25-900	17.5 ^{+1.46} _{-1.46}	4.24 ^{+0.39} _{-0.39}	SN	(13),(8)
081121	2.512	41.99 ± 8.51	-	Band	160.94 ^{+14.45} _{-14.45}	-0.44	-2.1	14.8 ± 0.42	2.19 ± 0.28	10-10000	2850 ^{+80.7} _{-80.7}	1480 ⁺¹⁹² ₋₁₉₂	-	(12)
081221	2.26	29.7 ± 0.41	-	CPL	88.4 ^{+1.11} _{-1.11}	-0.86	-	28.7 ± 0.23	2.08 ± 0.1	10-10000	3850 ^{+31.1} _{-31.1}	908 ⁺⁴⁵ ₋₄₅	-	(12)
081222	2.77	18.88 ± 2.32	-	Band	147.21 ^{+8.43} _{-8.43}	-0.84	-2.3	12.1 ± 0.34	1.85 ± 0.13	10-10000	2550 ^{+72.6} _{-72.6}	1480 ⁺¹⁰² ₋₁₀₂	-	(12)
090323	3.57	133.89 ± 0.57	-	SBPL	397.51 ^{+62.33} _{-62.33}	-1.24	-2.13	128.67 ± 1.2	2.69 ± 0.2	10-10000	44600 ⁺⁴¹⁶ ₋₄₁₆	4250 ⁺³²¹ ₋₃₂₁	-	(12)
090328	0.736	61.7 ± 1.81	-	CPL	711.34 ^{+39.28} _{-39.28}	-1.1	-	52.5 ± 0.6	5.41 ± 0.32	10-10000	1010 ^{+11.5} _{-11.5}	181 ^{+10.7} _{-10.7}	-	(12)
090423	8.26	7.17 ± 2.42	-	CPL	71.49 ^{+8.7} _{-8.7}	-0.65	-	0.57 ± 0.06	0.29 ± 0.08	10-10000	588 ^{+58.9} _{-58.9}	2730 ⁺⁷⁸⁸ ₋₇₈₈	-	(12)
090424	0.544	14.14 ± 0.26	-	Band	160 ^{+3.98} _{-3.98}	-1.02	-2.76	47 ± 0.53	14.32 ± 0.23	10-10000	418 ^{+4.74} _{-4.74}	196 ^{+3.17} _{-3.17}	-	(12)
090510	0.903	0.96 ± 0.14	-	CPL	4727.06 ^{+348.98} _{-348.98}	-0.86	-	4.42 ± 0.11	15.81 ± 0.61	10-10000	391 ^{+9.28} _{-9.28}	2660 ⁺¹⁰³ ₋₁₀₃	-	(12)
090516	4.109	123.14 ± 2.06	-	CPL	159.36 ^{+15.51} _{-15.51}	-1.47	-	27.4 ± 0.91	0.69 ± 0.13	10-10000	9350 ⁺³⁶⁷ ₋₃₆₇	1430 ⁺²⁷⁹ ₋₂₇₉	-	(12)
090618	0.54	112.39 ± 1.09	1415.31 ± 118.45	Band	149.04 ^{+3.29} _{-3.29}	-1.11	-2.24	234.41 ± 1.51	8.75 ± 0.55	10-10000	2820 ^{+15.5} _{-15.5}	139 ^{+8.66} _{-8.66}	-	(12)
090902B	1.822	19.33 ± 0.29	-	SBPL	789.1 ^{+59.14} _{-59.14}	-1.09	-4.86	279.38 ± 1.13	27.13 ± 0.52	10-10000	31700 ⁺¹²⁸ ₋₁₂₈	8680 ⁺¹⁶⁶ ₋₁₆₆	-	(12)
090926	2.1062	13.76 ± 0.29	-	SBPL	301.39 ^{+12.59} _{-12.59}	-0.98	-2.31	152.89 ± 0.68	25.83 ± 0.38	10-10000	21900 ^{+97.5} _{-97.5}	11500 ⁺¹⁷⁰ ₋₁₇₀	-	(12)
090926B	1.24	64 ± 1.56	-	CPL	84.8 ^{+2.05} _{-2.05}	0.16	-	7.57 ± 0.17	0.53 ± 0.11	10-10000	311 ^{+6.9} _{-6.9}	48.4 ^{+10.5} _{-10.5}	-	(12)
090927	1.37	0.51 ± 0.23	-	CPL	175.81 ^{+41.39} _{-41.39}	-0.64	-	0.21 ± 0.04	0.85 ± 0.14	10-10000	10.6 ^{+2.01} _{-2.01}	101 ^{+16.8} _{-16.8}	-	(12)
091003	0.8969	20.22 ± 0.36	-	CPL	432.21 ^{+21.1} _{-21.1}	-1.1	-	36 ± 0.56	8.19 ± 0.39	10-10000	882 ^{+13.7} _{-13.7}	381 ^{+18.1} _{-18.1}	-	(12)

Table 1 continued

Table 1 (continued)

<i>G</i> RB	<i>z</i>	<i>T</i> ₉₀ (s)	<i>T</i> ₃₁ (ms)	<i>model</i>	<i>E</i> _p (keV)	α	β	<i>S</i> _{γ,6} (erg cm ⁻²)	<i>F</i> _{p,-6} (erg cm ⁻² s ⁻¹)	<i>E</i> _{range}	<i>E</i> _{iso,50} (erg)	<i>I</i> _{iso,50} (erg s ⁻¹)	Ass.	Ref.
091020	1.71	24.26 ± 7.97	-	CPL	243.84 ^{+27.47} _{-5.47}	-1.26	-	8.01 ± 0.4	1.24 ± 0.15	10-1000	662 ^{+33.3} _{-33.3}	277 ^{+34.1} _{-34.1}	-	(12)
091024	1.092	450.57 ± 2.36	-	Band	162.5 ^{+9.99} _{-9.99}	-0.84	-2.15	54.1 ± 1.52	0.93 ± 0.2	10-1000	2350 ^{+66.1} _{-66.1}	84.3 ^{+18.1} _{-18.1}	-	(12)
091127	0.49	8.7 ± 0.57	94.2 ± 53.86	SBPL	32.75 ^{+4.43} _{-4.43}	-1.29	-2.23	18.3 ± 0.21	7.03 ± 0.15	10-1000	161 ^{+1.8} _{-1.8}	92 ^{+1.98} _{-1.98}	-	(12)
091208B	1.063	12.48 ± 5.02	-	Band	44.73 ^{+12.76} _{-12.76}	-0.62	-1.92	7.69 ± 0.29	3.16 ± 0.15	10-1000	350 ^{+13.3} _{-13.3}	297 ^{+13.7} _{-13.7}	-	(12)
100117A	0.92	0.26 ± 0.83	-	CPL	325.43 ^{+51.09} _{-51.09}	-0.1	-	0.37 ± 0.06	2.1 ± 0.23	10-1000	8.46 ^{+1.29} _{-1.29}	91.6 ^{+9.88} _{-9.88}	-	(12)
100206A	0.4068	0.18 ± 0.07	-	CPL	531.82 ^{+71.71} _{-71.71}	-0.4	-	0.97 ± 0.06	8.33 ± 0.38	10-1000	4.61 ^{+0.29} _{-0.29}	55.7 ^{+2.56} _{-2.56}	-	(12)
100414A	1.368	26.5 ± 2.07	-	CPL	668.15 ^{+14.63} _{-14.63}	-0.63	-	91.9 ± 0.66	9.01 ± 0.34	10-1000	5740 ⁺⁴¹ ₋₄₁	1330 ^{+49.6} _{-49.6}	-	(12)
100615A	1.398	37.38 ± 0.98	-	Band	53.55 ^{+7.5} _{-7.5}	-0.91	-1.8	13.3 ± 0.32	1.16 ± 0.11	10-1000	1110 ^{+26.5} _{-26.5}	232 ⁺²² ₋₂₂	-	(12)
100625A	0.452	0.24 ± 0.28	28.27 ± 4.19	CPL	483.19 ^{+63.32} _{-63.32}	-0.59	-	1.27 ± 0.1	4.69 ± 0.72	10-1000	7.37 ^{+0.55} _{-0.55}	39.5 ^{+6.06} _{-6.06}	-	(12)
100728A	1.567	165.38 ± 2.9	-	SBPL	232.06 ^{+13.34} _{-13.34}	-0.72	-2.48	124.54 ± 1.28	2.57 ± 0.24	10-1000	9850 ⁺¹⁰¹ ₋₁₀₁	521 ^{+47.8} _{-47.8}	-	(12)
100728B	2.106	10.24 ± 1.85	-	CPL	153.35 ^{+18.46} _{-18.46}	-1.01	-	2.68 ± 0.19	0.87 ± 0.13	10-1000	311 ^{+21.5} _{-21.5}	313 ^{+47.2} _{-47.2}	-	(12)
100814A	1.44	150.53 ± 1.62	-	CPL	146.68 ^{+6.75} _{-6.75}	-0.4	-	12.5 ± 0.43	0.84 ± 0.17	10-1000	685 ^{+23.3} _{-23.3}	112 ^{+22.8} _{-22.8}	-	(12)
100816A	0.8049	2.05 ± 0.23	137.06 ± 7.38	CPL	140.07 ^{+6.07} _{-6.07}	-0.37	-	3.35 ± 0.11	2.34 ± 0.13	10-1000	58.1 ^{+1.91} _{-1.91}	73.1 ^{+3.99} _{-3.99}	-	(12), This work
100906A	1.727	110.59 ± 2.83	-	Band	74.91 ^{+24.27} _{-24.27}	-0.93	-1.86	26.1 ± 0.69	1.29 ± 0.22	10-1000	3000 ^{+78.8} _{-78.8}	719 ^{+68.6} _{-68.6}	-	(12)
101213A	0.414	45.06 ± 1.95	-	CPL	342.95 ^{+30.26} _{-30.26}	-0.95	-	13.1 ± 0.6	1.37 ± 0.36	10-1000	60.8 ^{+2.79} _{-2.79}	9.01 ^{+2.36} _{-2.36}	-	(12)
101219B	0.55	51.01 ± 1.78	-	CPL	82.6 ^{+4.61} _{-4.61}	0.08	-	2.2 ± 0.11	0.26 ± 0.07	10-1000	17.5 ^{+0.9} _{-0.9}	3.23 ^{+0.86} _{-0.86}	-	(12)
110106B	0.618	35.52 ± 3.61	-	CPL	130.71 ^{+14.49} _{-14.49}	-0.94	-	1.97 ± 0.17	0.45 ± 0.12	10-1000	20.8 ^{+1.77} _{-1.77}	7.73 ^{+1.98} _{-1.98}	-	(12)
110213A	1.46	34.31 ± 1.64	-	CPL	112.57 ^{+11.82} _{-11.82}	-1.56	-	10.4 ± 0.43	1.64 ± 0.18	10-1000	737 ^{+30.6} _{-30.6}	286 ^{+30.6} _{-30.6}	-	(12)
110402A	0.854	35.65 ± 1.46	-	CPL	932.89 ^{+278.31} _{-278.31}	-1.33	-	7.39 ± 0.04	4.83 ± 0.41	10-1000	218 ^{+13.9} _{-13.9}	264 ^{+22.5} _{-22.5}	-	(12)
110731A	2.83	7.49 ± 0.57	-	SBPL	289.29 ^{+61.6} _{-61.6}	-1.04	-2.93	22.3 ± 0.38	5.26 ± 0.38	10-1000	4680 ^{+80.2} _{-80.2}	4230 ⁺³⁰⁷ ₋₃₀₇	-	(12)
110818A	3.36	67.07 ± 3.92	-	CPL	314.95 ^{+54.65} _{-54.65}	-1.19	-	6.3 ± 0.45	0.69 ± 0.21	10-1000	1700 ⁺¹²² ₋₁₂₂	811 ⁺²⁵⁰ ₋₂₅₀	-	(12)
111107A	2.893	12.03 ± 0.92	-	CPL	263.74 ^{+76.84} _{-76.84}	-1.28	-	1.86 ± 0.27	0.6 ± 0.23	10-1000	394 ^{+57.6} _{-57.6}	491 ⁺¹⁹¹ ₋₁₉₁	-	(12)
111117A	2.211	0.43 ± 0.08	2.41 ± 1	CPL	543.62 ^{+102.96} _{-102.96}	-0.5	-	0.68 ± 0.06	3.42 ± 0.33	10-1000	93.9 ^{+8.29} _{-8.29}	1510 ⁺¹⁴⁷ ₋₁₄₇	-	(12),(8)
111209A	0.677	6390 ± 630	-	CPL	310 ⁺⁵³ ₋₅₃	-1.31	-	486 ± 61	0.18 ± 0.02	20-1400	6730 ⁺⁸⁴⁵ ₋₈₄₅	4.27 ^{+0.43} _{-0.43}	-	(14)
111228A	0.714	99.84 ± 2.11	242.67 ± 124.02	Band	26.54 ^{+1.37} _{-1.37}	-1.58	-2.45	15.5 ± 0.38	1.52 ± 0.1	10-1000	334 ^{+8.07} _{-8.07}	56.2 ^{+3.54} _{-3.54}	-	(12),(8)
120119A	1.728	55.3 ± 6.23	-	Band	182.76 ^{+10.45} _{-10.45}	-0.95	-2.37	39.4 ± 0.55	2.97 ± 0.23	10-1000	3720 ^{+52.3} _{-52.3}	765 ^{+58.4} _{-58.4}	-	(12)
120326A	1.798	11.78 ± 1.81	-	SBPL	43.24 ^{+10.05} _{-10.05}	-0.92	-2.4	3.84 ± 0.17	0.76 ± 0.09	10-1000	382 ^{+17.3} _{-17.3}	212 ^{+25.3} _{-25.3}	-	(12)
120624B	2.1974	271.36 ± 4.58	-	SBPL	592.78 ^{+76.33} _{-76.33}	-1.02	-2.22	196.15 ± 1.54	5.14 ± 0.3	10-1000	33800 ⁺²⁶⁶ ₋₂₆₆	2840 ⁺¹⁶⁸ ₋₁₆₈	-	(12)
120711A	1.405	44.03 ± 0.72	-	Band	1317.52 ^{+42.26} _{-42.26}	-0.98	-2.8	197.58 ± 1	12.66 ± 0.8	10-1000	18800 ^{+95.2} _{-95.2}	2900 ⁺¹⁸² ₋₁₈₂	-	(12)
120712A	4.1745	22.53 ± 5.43	-	CPL	171.67 ^{+11.94} _{-11.94}	-0.33	-	3.52 ± 0.18	0.77 ± 0.16	10-1000	1220 ^{+62.8} _{-62.8}	1390 ⁺²⁷⁹ ₋₂₇₉	-	(12)
120716A	2.486	226.05 ± 1.06	-	CPL	131.6 ^{+5.29} _{-5.29}	-0.96	-	12.9 ± 0.3	1.5 ± 0.14	10-1000	2010 ^{+46.7} _{-46.7}	814 ^{+78.3} _{-78.3}	-	(12)
120811C	2.671	14.34 ± 6.56	-	CPL	60.81 ^{+3.73} _{-3.73}	-0.93	-	3.29 ± 0.15	0.82 ± 0.17	10-1000	625 ^{+28.5} _{-28.5}	571 ⁺¹¹⁸ ₋₁₁₈	-	(12)
120907A	0.97	5.76 ± 1.78	-	CPL	120.71 ^{+22.14} _{-22.14}	-0.79	-	0.69 ± 0.11	0.71 ± 0.18	10-1000	18.1 ^{+2.85} _{-2.85}	36.7 ^{+9.44} _{-9.44}	-	(12)
120909A	3.93	112.07 ± 10.42	-	Band	199.65 ^{+24.28} _{-24.28}	-0.84	-1.93	18.1 ± 0.57	0.73 ± 0.17	10-1000	7200 ⁺²²⁸ ₋₂₂₈	1430 ⁺³²⁹ ₋₃₂₉	-	(12)
121128A	2.2	17.34 ± 0.92	-	SBPL	56.49 ^{+8.52} _{-8.52}	-0.91	-2.48	9.95 ± 0.33	2.11 ± 0.19	10-1000	1370 ⁺⁴⁶ ₋₄₆	932 ^{+83.7} _{-83.7}	-	(12)
121211A	1.023	5.63 ± 1.72	-	CPL	98.04 ^{+10.34} _{-10.34}	-0.22	-	0.49 ± 0.05	0.39 ± 0.1	10-1000	14 ^{+1.42} _{-1.42}	22.5 ^{+5.6} _{-5.6}	-	(12)
130215A	0.597	143.75 ± 13.03	-	Band	209.95 ^{+42.31} _{-42.31}	-1.06	-1.61	17.6 ± 0.43	0.9 ± 0.2	10-1000	384 ^{+9.37} _{-9.37}	31.4 ^{+6.99} _{-6.99}	-	(12)
130420A	1.297	104.96 ± 8.81	-	CPL	56.98 ^{+3.02} _{-3.02}	-1.12	-	5.76 ± 0.21	0.53 ± 0.12	10-1000	308 ^{+11.1} _{-11.1}	65.3 ^{+14.9} _{-14.9}	-	(12)
130427A	0.3399	138.24 ± 3.24	1084.86 ± 123.23	Band	824.99 ^{+5.45} _{-5.45}	-1.02	-2.83	1411.72 ± 1.82	305.44 ± 2.55	10-1000	6370 ^{+8.22} _{-8.22}	1850 ^{+15.4} _{-15.4}	-	(12),(8)
130518A	2.488	48.58 ± 0.92	-	SBPL	419.83 ^{+57.72} _{-57.72}	-0.97	-2.11	95.5 ± 0.73	11.05 ± 0.37	10-1000	19300 ⁺¹⁴⁷ ₋₁₄₇	7780 ⁺²⁶⁴ ₋₂₆₄	-	(12)
130603B	0.36	0.07 ± 0.01	9.6 ± 2.49	CPL	607 ⁺⁶¹ ₋₆₁	-0.67	-	5.72 ± 0.29	81.3 ± 5.2	10-10000	18.4 ^{+0.93} _{-0.93}	356 ^{+22.8} _{-22.8}	KN	(1),(8)
130610A	2.092	21.76 ± 1.64	-	CPL	284.99 ^{+61.61} _{-61.61}	-1.58	-	5.72 ± 0.47	0.53 ± 0.16	10-1000	791 ^{+65.4} _{-65.4}	227 ^{+66.8} _{-66.8}	-	(12)

Table 1 continued

Table 1 (continued)

<i>G</i> RB	<i>z</i>	<i>T</i> ₉₀ (s)	<i>T</i> ₃₁ (ms)	<i>model</i>	<i>E</i> _p (keV)	α	β	<i>S</i> _{γ-6} (erg cm ⁻²)	<i>F</i> _{p,-6} (erg cm ⁻² s ⁻¹)	<i>E</i> _{range}	<i>E</i> _{iso,50} (erg)	<i>I</i> _{iso,50} (erg s ⁻¹)	Ass.	Ref.
130612A	2.006	7.42 ± 6.19	-	CPL	57.73 ⁺¹⁰ ₋₁₀	-1.37	-	0.46 ± 0.05	0.25 ± 0.07	10-1000	60.5 ^{+6.08} _{-6.08}	99.4 ^{+25.9} _{-25.9}	-	(12)
130702A	0.145	58.88 ± 6.19	-	CPL	15.17 ^{+0.98} _{-0.28}	1.6	-	3.67 ± 0.06	0.43 ± 0.12	10-1000	2.49 ^{+0.04} _{-0.04}	0.34 ^{+0.1} _{-0.1}	-	(12)
130831A	0.4791	17.53 ± 2.81	477.57 ± 62.02	CPL	54 ⁺⁹ ₋₉	-1.64	-	8.93 ± 0.4	2.32 ± 0.28	10-10000	74.8 ^{+3.35} _{-3.35}	28.7 ^{+3.47} _{-3.47}	SN	(1),(8)
130925A	0.347	6.4 ± 2.43	-	CPL	23.75 ^{+2.54} _{-2.54}	-0.69	-	0.42 ± 0.03	0.21 ± 0.06	10-1000	1.74 ^{+0.11} _{-0.11}	1.19 ^{+0.33} _{-0.33}	-	(12)
130925A	0.347	215.56 ± 1.81	-	CPL	84.53 ^{+1.61} _{-1.61}	-1.66	-	86.7 ± 0.72	0.96 ± 0.11	10-1000	348 ^{+2.88} _{-2.88}	5.17 ^{+0.57} _{-0.57}	-	(12)
131004A	0.717	1.15 ± 0.59	130 ± 20	CPL	117.91 ^{+24.21} _{-24.21}	-1.36	-	0.44 ± 0.05	0.79 ± 0.14	10-1000	1050 ^{+44.9} _{-44.9}	21.4 ^{+3.73} _{-3.73}	-	(12)
131011A	1.874	77.06 ± 3	-	CPL	274.10 ^{+24.27} _{-24.27}	-0.96	-	11.3 ± 0.48	1.02 ± 0.2	10-1000	60.5 ^{+6.08} _{-6.08}	99.4 ^{+25.9} _{-25.9}	-	(12)
131105A	1.686	112.64 ± 0.46	-	CPL	266.11 ^{+15.38} _{-15.38}	-1.26	-	24.6 ± 0.58	1.51 ± 0.15	10-1000	1990 ^{+47.3} _{-47.3}	327 ^{+31.9} _{-31.9}	-	(12)
131108A	2.4	18.18 ± 0.57	-	SBPL	318.13 ^{+40.22} _{-40.22}	-1.04	-2.42	36.2 ± 0.42	6.81 ± 0.29	10-1000	6330 ^{+73.1} _{-73.1}	4040 ⁺¹⁷⁵ ₋₁₇₅	-	(12)
131231A	0.642	31.23 ± 0.57	-	Band	178.09 ^{+4.03} _{-4.03}	-1.22	-2.3	153.8 ± 0.67	9.51 ± 0.31	10-1000	2230 ^{+9.73} _{-9.73}	226 ^{+7.33} _{-7.33}	-	(12)
140206A	2.73	146.69 ± 4.42	-	SBPL	537.61 ^{+153.06} _{-153.06}	-1.45	-2.05	127.71 ± 0.89	6.41 ± 0.22	10-1000	30900 ⁺²¹⁵ ₋₂₁₅	5790 ⁺¹⁹⁵ ₋₁₉₅	-	(12)
140213A	1.2076	18.62 ± 0.72	-	Band	86.15 ^{+4.1} _{-4.1}	-1.13	-2.25	23.9 ± 0.4	3.92 ± 0.19	10-1000	1210 ^{+20.1} _{-20.1}	437 ^{+21.2} _{-21.2}	-	(12)
140304A	5.283	31.23 ± 8.72	-	CPL	141.44 ^{+18.46} _{-18.46}	-0.89	-	1.92 ± 0.16	0.42 ± 0.08	10-1000	999 ^{+84.3} _{-84.3}	1380 ⁺²⁶⁶ ₋₂₆₆	-	(12)
140423A	3.26	95.23 ± 11.59	-	Band	116.17 ^{+15.89} _{-15.89}	-0.55	-1.79	21.5 ± 0.6	0.79 ± 0.15	10-1000	6880 ⁺¹⁹³ ₋₁₉₃	1070 ⁺²¹¹ ₋₂₁₁	-	(12)
140506A	0.889	64.13 ± 2.01	-	CPL	197.58 ^{+26.29} _{-26.29}	-1.18	-	4.63 ± 0.33	2.78 ± 0.33	10-1000	105 ^{+7.48} _{-7.48}	119 ^{+14.1} _{-14.1}	-	(12)
140508A	1.027	44.29 ± 0.23	-	Band	257.4 ^{+12.12} _{-12.12}	-1.18	-2.32	63.1 ± 0.8	11.95 ± 0.59	10-1000	2370 ^{+30.1} _{-30.1}	910 ^{+44.6} _{-44.6}	-	(12)
140512A	0.725	147.97 ± 2.36	-	CPL	691.86 ^{+57.05} _{-57.05}	-1.23	-	45.5 ± 0.73	2.81 ± 0.23	10-1000	852 ^{+13.7} _{-13.7}	90.6 ^{+7.41} _{-7.41}	-	(12)
140606B	0.384	22.78 ± 2.06	-	CPL	577.63 ^{+102.84} _{-102.84}	-1.24	-	9.57 ± 0.43	2.79 ± 0.23	10-1000	45 ⁺² ₋₂	18.2 ^{+1.51} _{-1.51}	-	(12)
140620A	2.04	45.83 ± 12.13	-	CPL	130.24 ^{+12.24} _{-12.24}	-1.29	-	6.17 ± 0.29	0.79 ± 0.15	10-1000	725 ^{+33.5} _{-33.5}	281 ⁺⁵² ₋₅₂	-	(12)
140623A	1.92	111.1 ± 4	-	CPL	317.03 ^{+82.62} _{-82.62}	-1.42	-	3.36 ± 0.35	0.47 ± 0.14	10-1000	370 ^{+38.4} _{-38.4}	151 ^{+45.3} _{-45.3}	-	(12)
140703A	3.14	83.97 ± 3	-	CPL	218.59 ^{+23.22} _{-23.22}	-1.28	-	9.04 ± 0.42	0.63 ± 0.11	10-1000	2180 ⁺¹⁰⁰ ₋₁₀₀	628 ⁺¹¹⁰ ₋₁₁₀	-	(12)
140801A	1.32	7.17 ± 0.57	-	CPL	121.11 ^{+2.11} _{-2.11}	-0.4	-	12 ± 0.16	3.84 ± 0.18	10-1000	560 ^{+7.24} _{-7.24}	416 ^{+19.1} _{-19.1}	-	(12)
140808A	3.29	4.48 ± 0.36	-	CPL	125.43 ^{+6.15} _{-6.15}	-0.49	-	3.22 ± 0.11	1.18 ± 0.14	10-1000	773 ^{+27.1} _{-27.1}	1210 ⁺¹⁴⁸ ₋₁₄₈	-	(12)
140907A	1.21	35.84 ± 5.47	-	CPL	137.9 ^{+7.81} _{-7.81}	-1.01	-	6.23 ± 0.22	0.58 ± 0.13	10-1000	257 ^{+9.08} _{-9.08}	53 ^{+11.9} _{-11.9}	-	(12)
141004A	0.573	2.56 ± 0.61	276.05 ± 48.98	CPL	181.77 ^{+5.61} _{-5.61}	-1.6	-	1.42 ± 0.18	1.57 ± 0.17	10-1000	15.1 ^{+1.91} _{-1.91}	26.2 ^{+2.85} _{-2.85}	-	(12),(8)
141028A	2.33	31.49 ± 2.43	-	Band	293.1 ^{+17.98} _{-17.98}	-0.84	-1.97	39.9 ± 0.4	4.09 ± 0.26	10-1000	7470 ^{+75.5} _{-75.5}	2550 ⁺¹⁶⁴ ₋₁₆₄	-	(12)
141220A	1.3185	7.62 ± 0.92	-	CPL	178.3 ^{+9.11} _{-9.11}	-0.82	-	5.55 ± 0.18	1.96 ± 0.18	10-1000	262 ^{+8.36} _{-8.36}	215 ^{+19.8} _{-19.8}	-	(12)
141221A	1.452	23.81 ± 1.72	-	CPL	182.07 ^{+31.97} _{-31.97}	-1.18	-	2.86 ± 0.26	0.96 ± 0.16	10-1000	171 ^{+15.7} _{-15.7}	140 ^{+23.9} _{-23.9}	-	(12)
141225A	0.915	56.32 ± 4.89	-	CPL	257.58 ^{+26.96} _{-26.96}	-0.6	-	5.91 ± 0.37	0.78 ± 0.2	10-1000	134 ^{+8.32} _{-8.32}	33.7 ^{+8.59} _{-8.59}	-	(12)
150101B	0.134	0.08 ± 0.93	20.91 ± 3.4	CPL	125.11 ^{+48.57} _{-48.57}	-1.36	-	0.08 ± 0.02	0.87 ± 0.11	10-1000	0.04 ^{+0.01} _{-0.01}	0.47 ^{+0.06} _{-0.06}	-	(12),(8)
150301B	1.5169	13.31 ± 1.56	-	CPL	225.43 ^{+27.53} _{-27.53}	-1.12	-	4.04 ± 0.25	0.78 ± 0.13	10-1000	258 ^{+15.7} _{-15.7}	125 ^{+20.6} _{-20.6}	-	(12)
150314A	1.758	10.69 ± 0.14	-	Band	347.16 ^{+7.9} _{-7.9}	-0.68	-2.6	88.9 ± 0.61	16.3 ± 0.44	10-1000	8670 ^{+59.6} _{-59.6}	4380 ⁺¹¹⁸ ₋₁₁₈	-	(12)
150403A	2.06	22.27 ± 0.81	-	Band	428.74 ^{+21.06} _{-21.06}	-0.87	-2.11	64.2 ± 0.64	8.2 ± 0.45	10-1000	9700 ^{+96.1} _{-96.1}	3790 ⁺²⁰⁸ ₋₂₀₈	-	(12)
150514A	0.807	10.81 ± 1.07	-	CPL	78.45 ^{+4.22} _{-4.22}	-1.36	-	4.57 ± 0.13	1.52 ± 0.1	10-1000	96.4 ^{+2.72} _{-2.72}	58 ^{+3.93} _{-3.93}	-	(12)
150727A	0.313	49.41 ± 3.97	-	CPL	208.53 ^{+17.14} _{-17.14}	-0.35	-	5.9 ± 0.32	0.77 ± 0.2	10-1000	14.3 ^{+0.78} _{-0.78}	2.43 ^{+0.64} _{-0.64}	-	(12)
150818A	0.282	184.26 ± 18.43	568.98 ± 99.37	CPL	111 ⁺⁵³ ₋₅₃	-1.77	-	8.1 ± 1.09	0.55 ± 0.15	15-15000	23 ^{+3.09} _{-3.09}	2 ^{+0.54} _{-0.54}	SN	(16),(8)
150821A	0.755	103.43 ± 5.75	-	Band	281.22 ^{+17.11} _{-17.11}	-1.24	-2.13	71.1 ± 0.83	1.86 ± 0.19	10-1000	1600 ^{+18.6} _{-18.6}	73.3 ^{+7.6} _{-7.6}	-	(12)
151027A	0.81	123.39 ± 1.15	-	SBPL	304.98 ^{+267.4} _{-267.4}	-1.35	-2.04	17.3 ± 0.45	1.67 ± 0.18	10-1000	466 ^{+12.2} _{-12.2}	81.5 ^{+8.53} _{-8.53}	-	(12)
160509A	1.17	369.67 ± 0.81	-	Band	355.19 ^{+9.88} _{-9.88}	-1.02	-2.23	204.14 ± 1.11	14.8 ± 0.41	10-1000	10500 ^{+57.1} _{-57.1}	1650 ^{+45.8} _{-45.8}	-	(12)
160625B	1.406	453.39 ± 0.57	-	SBPL	510.94 ^{+27.12} _{-27.12}	-1.02	-2.1	668.22 ± 1.99	48.14 ± 0.86	10-1000	53200 ⁺¹⁵⁸ ₋₁₅₈	9220 ⁺¹⁶⁵ ₋₁₆₅	-	(12)
160629A	3.332	64.77 ± 0.92	-	CPL	290.75 ^{+19.27} _{-19.27}	-1.03	-	18.9 ± 0.61	1.13 ± 0.15	10-1000	4830 ⁺¹⁵⁶ ₋₁₅₆	1250 ⁺¹⁶⁶ ₋₁₆₆	-	(12)
160804A	0.736	131.59 ± 21.72	-	CPL	75.85 ^{+2.81} _{-2.81}	-1.09	-	12.4 ± 0.29	0.48 ± 0.11	10-1000	203 ^{+4.65} _{-4.65}	13.7 ^{+3.11} _{-3.11}	-	(12)

Table 1 continued

Table 1 (continued)

<i>GRB</i>	<i>z</i>	<i>T</i> ₉₀ (s)	<i>τ</i> ₃₁ (ms)	<i>model</i>	<i>E</i> _p (keV)	α	$S_{\gamma,-6}$ (erg cm ⁻²)	$F_{p,-6}$ (erg cm ⁻² s ⁻¹)	<i>E</i> _{range}	<i>E</i> _{iso,50} (erg)	<i>I</i> _{iso,50} (erg s ⁻¹)	<i>Ass.</i>	<i>Ref.</i>
160821B	0.16	1.09 ± 0.98	26.53 ± 0.71	CPL	91.97 ^{+27.87} _{-26.58}	-1.4	0.17 ± 0.02	0.65 ± 0.08	10-1000	0.12 ^{+0.02} _{-0.02}	0.54 ^{+0.07} _{-0.07}	-	(12),(8)
161001A	0.67	2.24 ± 0.23	32.57 ± 5.93	CPL	373.17 ^{+58.58} _{-58.58}	-0.94	2.36 ± 0.19	3.27 ± 0.23	10-1000	30.2 ^{+2.4} _{-2.4}	69.8 ^{+4.97} _{-4.97}	-	(12),This work
161014A	2.823	36.61 ± 1.49	-	CPL	169.79 ^{+12.78} _{-12.78}	-0.76	5.08 ± 0.26	1.14 ± 0.16	10-1000	950 ^{+48.8} _{-48.8}	812 ⁺¹¹¹ ₋₁₁₁	-	(12)
161017A	2.013	37.89 ± 10.86	-	CPL	277.18 ^{+40.6} _{-40.6}	-1.09	5.79 ± 0.4	1.4 ± 0.3	10-1000	626 ^{+42.7} _{-42.7}	455 ⁺⁹⁷ ₋₉₇	-	(12)
161117A	1.549	122.18 ± 0.66	-	CPL	85.04 ^{+1.72} _{-1.72}	-0.87	30.8 ± 0.4	1.08 ± 0.17	10-1000	2080 ^{+26.9} _{-26.9}	186 ^{+29.2} _{-29.2}	-	(12)
161219A	0.645	36.1 ± 0.72	-	CPL	214.04 ^{+22.38} _{-22.38}	-1.16	8.85 ± 0.44	1.41 ± 0.17	10-1000	104 ^{+5.12} _{-5.12}	27.1 ^{+3.29} _{-3.29}	-	(12)
161219B	0.1475	7.04 ± 0.7	-	CPL	94 ⁺¹⁹ ₋₁₂	-1.51	2.69 ± 0.3	0.88 ± 0.16	15-15000	1.81 ^{+0.2} _{-0.2}	0.68 ^{+0.12} _{-0.12}	SN	(16)
170113A	1.968	49.15 ± 4.14	-	CPL	106.56 ^{+36.71} _{-36.71}	-1.69	1.74 ± 0.3	0.5 ± 0.17	10-1000	234 ^{+39.7} _{-39.7}	198 ^{+67.7} _{-67.7}	-	(12)
170214A	2.53	122.88 ± 0.72	-	SBPL	402.03 ^{+27.05} _{-27.05}	-1.06	197.64 ± 1.08	4.75 ± 0.37	10-1000	40000 ⁺²¹⁸ ₋₂₆₂	3390 ⁺²⁶² ₋₂₆₂	-	(12)
170607A	0.557	20.93 ± 2.1	-	CPL	145.17 ^{+11.88} _{-11.88}	-1.4	9.44 ± 0.32	1.73 ± 0.22	10-1000	87.6 ⁺³ ₋₃	25 ^{+3.24} _{-3.24}	-	(12)
170705A	2.01	22.78 ± 1.38	-	Band	97.88 ^{+7.64} _{-7.64}	-0.99	14.4 ± 0.43	2.64 ± 0.24	10-1000	1780 ^{+53.5} _{-53.5}	986 ^{+90.2} _{-90.2}	-	(12)
170817A	0.0093	2.05 ± 0.47	150 ± 15	CPL	215.09 ^{+54.22} _{-54.22}	0.14	0.14 ± 0.03	0.73 ± 0.18	10-1000	0.0003 ^{+0.0001} _{-0.0001}	0.0014 ^{+0.0003} _{-0.0003}	-	(12)
171010A	0.3285	107.27 ± 0.81	-	Band	137.66 ^{+1.43} _{-1.43}	-1.09	671.82 ± 1.66	15.7 ± 0.5	10-1000	2530 ^{+6.26} _{-6.26}	78.6 ^{+2.53} _{-2.53}	-	(12)
171205A	0.0368	216.9 ± 21.69	9560 ± 3130	CPL	111 ⁺²³ ₋₁₅	-0.78	7.43 ± 1.13	0.57 ± 0.15	15-15000	0.24 ^{+0.04} _{-0.04}	0.02 ^{+0.01} _{-0.01}	SN	(16),(8)
171222A	2.409	80.38 ± 4.62	-	CPL	203.5 ^{+3.44} _{-3.44}	-2.01	2.02 ± 0.1	0.42 ± 0.14	10-1000	564 ⁺⁵⁷ ₋₅₇	402 ⁺¹³² ₋₁₃₂	-	(12)
180618A	0.544	3.71 ± 0.58	3.26 ± 10.22	CPL	2507.58 ^{+917.74} _{-917.74}	-1.13	2.15 ± 0.14	3.78 ± 0.48	10-1000	42.6 ^{+2.82} _{-2.82}	116 ^{+14.8} _{-14.8}	-	(12),(8)
180620B	1.1175	46.72 ± 1.33	-	Band	175.63 ^{+49.79} _{-49.79}	-1.21	12.5 ± 0.34	2.03 ± 0.44	10-1000	817 ^{+22.5} _{-22.5}	281 ^{+60.5} _{-60.5}	-	(12)
180720B	0.654	48.9 ± 0.36	-	Band	636.04 ^{+15.43} _{-15.43}	-1.17	2.49 ± 0.145	32.45 ± 0.51	10-1000	5310 ^{+24.2} _{-24.2}	897 ⁺¹⁴ ₋₁₄	-	(12)
180728A	0.117	6.4 ± 0.36	-71.2 ± 32.08	Band	79.2 ^{+1.4} _{-1.4}	-1.54	56.5 ± 0.2	19.24 ± 0.36	10-1000	24.6 ^{+0.09} _{-0.09}	9.36 ^{+0.17} _{-0.17}	SN	(12),(8)
181201A	0.45	172 ± 17.2	-	Band	152 ⁺⁶ ₋₆	-1.25	-2.73	28.8 ± 3.4	20-10000	1180 ^{+35.7} _{-35.7}	248 ^{+29.3} _{-29.3}	SN	(17)
190114C	0.425	116.35 ± 2.56	745.25 ± 86.39	Band	998.6 ^{+11.9} _{-11.9}	-1.06	3.18	84.19 ± 0.97	10-1000	3010 ^{+6.11} _{-6.11}	904 ^{+10.4} _{-10.4}	-	(12),(8)
200826A	0.7481	1.14 ± 0.13	57.87 ± 0.5	Band	89.8 ^{+3.7} _{-3.7}	-0.41	4.8 ± 0.1	7 ± 0.22	10-1000	85 ^{+1.77} _{-1.77}	217 ^{+6.92} _{-6.92}	-	(12)
211023A	0.39	79.11 ± 0.57	-	Band	99 ⁺² ₋₂	-1.74	-2.55	2.91 ± 5.04	10-1000	629 ^{+3.97} _{-3.97}	23 ^{+39.7} _{-39.7}	-	(12)
211211A	0.076	34.31 ± 0.57	12 ± 10	Band	646.8 ^{+7.8} _{-7.8}	-1.3	-2.4	79.19 ± 1.19	10-1000	111 ^{+0.21} _{-0.21}	17.6 ^{+0.26} _{-0.26}	-	(12),(18)
211211A*	0.076	13 ± 1.3	10 ± 3	Band	687.1 ^{+11.55} _{-11.55}	-1	-2.36	111.32 ± 1.07	10-1000	83 ^{+0.32} _{-0.32}	26.4 ^{+0.4} _{-0.4}	-	(18)
211227A	0.228	82.5 ± 8.25	-	Band	192 ⁺⁴⁵ ₋₄₂	-1.34	-2.26	2 ± 0.4	15-1500	44.2 ^{+3.57} _{-3.57}	4.18 ^{+0.84} _{-0.84}	KN	(19)
211227A*	0.228	4 ± 0.4	-	CPL	400 ⁺¹²⁰⁰ ₋₂₀₀	-1.56	-	2.01 ± 0.19	15-1500	3.11 ^{+0.29} _{-0.29}	3.8 ^{+0.76} _{-0.76}	KN	(20)
230307A	0.065	34.56 ± 0.57	12.94 ± 0.01	CPL	936 ⁺³ ₋₃	-1.07	2950 ± 4	226.42 ± 3.93	10-1000	427 ^{+0.58} _{-0.58}	34.9 ^{+0.61} _{-0.61}	-	(12),This work
230812B	0.36	3.26 ± 0.09	-	Band	273 ⁺³ ₋₃	-0.8	-2.47	161.72 ± 1.52	10-1000	1070 ^{+0.08} _{-0.08}	932 ^{+8.78} _{-8.78}	-	(21)

References—(1)-Tsvetkova et al. (2017);(2)-Amati et al. (2002);(3)-Yamazaki et al. (2003);(4)-Goldstein et al. (2013);(5)-Sakamoto et al. (2004);(6)-Wiersema et al. (2008);(7)-Lien et al. (2010);(8)-Li et al. (2023);(9)-Kaneke et al. (2007);(10)-Zhu et al. (2023);(11)-Gebrels et al. (2006);(12)-von Kienlin et al. (2020);(13)-Bissaldi et al. (2008);(14)-Golonetkii et al. (2011);(15)-Stamatikos et al. (2013);(16)-Tsuetkova et al. (2013);(17)-Svinkin et al. (2018);(18)-Yang et al. (2022);(19)-Tsuetkova et al. (2022);(20)-Zhu et al. (2022);(21)-Robertis et al. (2023).

Table 2. The prompt emission parameters of peculiar GRBs

GRB	T_{90} (s)	model	E_p (keV)	α	β	$S_{\gamma,-6}$ (erg cm $^{-2}$)	F_p (ph cm $^{-2}$ s $^{-1}$)	HR	res ^a (ms)	τ_{31} (ms)	P_{EP}^b (%)	F_{HR}^b (%)	z_{ϵ}^c (%)	P_{ϵ}^d (%)	z_{EH}^e	P_{EH}^d (%)
Group A GRBs																
080816989	4.61 ± 0.45	CPL	1530 ± 224	-0.5	...	3.21 ± 0.15	9.27 ± 0.62	2.23	64	-110.17 ± 19.11	8.9	35.3	...	0	...	0
080828189	3.01 ± 3.33	CPL	118.9 ± 10.3	10.65	...	0.11 ± 0.02	5.62 ± 0.98	1.51	64	-134.49 ± 40.63	81	28.2	...	0	...	0
081006604	6.4 ± 0.92	CPL	653.6 ± 165.8	-0.43	...	1.72 ± 0.18	4.69 ± 1.2	1.23	256	...	62.3	83.1	...	0	...	0
090510325	7.42 ± 1.72	CPL	1957 ± 581	-0.63	...	1.84 ± 0.17	3.14 ± 1.21	1.18	256	...	18.6	88.6	...	0	...	0
090518080	2.05 ± 0.41	CPL	331.5 ± 122.1	-1.35	...	1 ± 0.16	9.75 ± 5.05	1.01	64	101.92 ± 24.86	17.9	19.3	2.727-10	20.4	...	0
090610648	6.14 ± 8.14	CPL	2000 ± 416	-0.79	...	1.89 ± 0.11	4.6 ± 0.74	2.81	128	-467.66 ± 179.86	11	38.8	...	0	...	0
100502061	2.24 ± 1.61	CPL	2739 ± 664	-0.75	...	0.69 ± 0.06	4.28 ± 1.17	0.81	128	-174.89 ± 119.58	0.2	28.1	...	0	...	0
100516369	2.11 ± 1.13	CPL	208.8 ± 57.4	-0.36	...	0.07 ± 0.02	5.09 ± 1.06	1.41	64	313.66 ± 114.63	36.5	13.3	...	0	...	0
100717372	5.95 ± 1.51	CPL	3994 ± 1288	-1.01	...	1.29 ± 0.09	7.57 ± 1.36	1.24	16	18.07 ± 5.35	2	79.9	...	0	...	0
100717446	2.43 ± 1.36	CPL	692.8 ± 192.3	-0.62	...	0.74 ± 0.06	5.56 ± 1.03	1.95	128	358.59 ± 53.72	7.5	10	...	0	...	0
100719825	3.07 ± 3.11	CPL	405.5 ± 102.5	-0.55	...	1.32 ± 0.2	4.57 ± 1.45	0.93	128	203.01 ± 119.59	33.5	46.7	4-8.455	9.5	...	0
100922625	4.35 ± 0.92	CPL	1338 ± 343	-0.56	...	1.19 ± 0.13	2.55 ± 1.03	0.8	256	-163.48 ± 92.23	10.1	72.5	...	0	...	0
101214748	2.24 ± 2.08	CPL	345.3 ± 100.5	-0.52	...	0.23 ± 0.05	7.41 ± 1.38	0.76	32	80.82 ± 33.56	21	29.1	...	0	...	0
110112934	2.3 ± 2.54	CPL	552.1 ± 138.3	-0.74	...	0.4 ± 0.06	8.22 ± 1.23	0.9	32	35.58 ± 157.44	10	28	...	0	...	0
110307972	2.3 ± 3.44	CPL	347.6 ± 57.9	0.42	...	0.49 ± 0.07	5.88 ± 0.98	1.91	256	-978.2 ± 55.71	22.2	8.9	...	0	...	0
110331604	3.2 ± 0.95	CPL	905 ± 201.1	-0.49	...	2.24 ± 0.15	4.01 ± 1.3	1.71	256	1041 ± 211.1	9.6	26.5	...	0	...	0
110401920	2.37 ± 1.27	CPL	1282 ± 366	-0.76	...	1.37 ± 0.09	10.81 ± 1.37	2.73	16	-65.3 ± 9.17	1.8	3.5	...	0	...	0
120114433	2.75 ± 1.57	CPL	240.8 ± 62.2	0.38	...	0.19 ± 0.06	3.78 ± 1.06	1.1	256	...	49.5	34	...	0	...	0
120219563	8.13 ± 0.43	CPL	1990 ± 750	-0.82	...	1.44 ± 0.13	2.6 ± 0.83	1.55	256	...	22.2	86.4	...	0	...	0
121220311	5.12 ± 0.81	CPL	739.5 ± 266.8	-0.67	...	0.97 ± 0.13	2.73 ± 0.93	1.13	128	257.38 ± 213.61	40.2	74.9	...	0	...	0
130112353	2.05 ± 1.56	CPL	548.3 ± 90.1	-0.71	...	1.22 ± 0.09	8.6 ± 1.17	1.23	32	226.49 ± 47.69	7.2	15.1	...	0	...	0
130518551	4.1 ± 2.57	CPL	980.5 ± 173.5	-0.83	...	4.03 ± 0.18	19.81 ± 1.08	1.45	8	-0.02 ± 0.82	15.9	51.4	...	0	...	0
131123543	3.14 ± 0.72	CPL	374.1 ± 82.9	-0.77	...	1 ± 0.16	6.65 ± 1.16	1.08	64	-320.91 ± 290.05	38.6	43.9	...	0	...	0
140216331	2.43 ± 0.59	CPL	779.2 ± 284.4	-0.84	...	1.08 ± 0.13	3.46 ± 1.04	1.98	128	...	5.9	9.6	...	0	...	0
140224382	2.3 ± 2.11	CPL	1329 ± 479	-0.99	...	2 ± 0.16	8.81 ± 1.35	0.96	16	-13.52 ± 17.94	1.5	26.7	...	0	...	0
140619475	2.82 ± 0.81	CPL	1479 ± 261	-0.26	...	1.67 ± 0.09	5.28 ± 0.75	3.21	128	208.47 ± 76.18	2.2	3.5	...	0	...	0
140831374	3.58 ± 2.57	CPL	836.8 ± 313.9	-1.06	...	1.58 ± 0.16	6.08 ± 1.4	1.15	64	21.97 ± 73.44	15.1	51.5	...	0	...	0
140930134	3.26 ± 1.62	CPL	797.5 ± 317.9	-0.69	...	1.03 ± 0.11	4.73 ± 0.89	1.7	256	...	12.9	27.8	...	0	...	0
141102536	2.62 ± 0.33	CPL	639.4 ± 99.1	-0.7	...	1.61 ± 0.08	15.59 ± 1.24	1.34	8	-9.94 ± 1.51	10.9	24.6	...	0	...	0
141222298	2.75 ± 0.26	CPL	3290 ± 956	-1.55	...	9.25 ± 0.16	121.02 ± 2.62	0.45	8	1.56 ± 0.04	0.3	43.2	...	0	...	0
150228845	4.13 ± 1.06	CPL	1184 ± 146.7	-0.82	...	7.48 ± 0.17	17.76 ± 1.32	1.6	16	80.15 ± 27.26	11.2	47.1	1.727-8.182	35.9	...	0
150828901	2.05 ± 1.78	CPL	589.9 ± 209	-0.95	...	0.56 ± 0.11	3.01 ± 0.9	2.59	256	...	6.3	2.7	...	0	...	0
160219289	3.52 ± 0.18	CPL	547.6 ± 133	-0.87	...	1.48 ± 0.16	19.19 ± 1.11	1.18	16	77.07 ± 30.88	29.3	49	...	0	...	0
160628136	5.89 ± 2.43	CPL	943 ± 307	-0.94	...	2.01 ± 0.16	6.13 ± 1.29	1.35	128	...	37.6	77.1	...	0	...	0
160818230	2.18 ± 0.91	CPL	256.7 ± 50.8	-0.4	...	0.44 ± 0.06	8.18 ± 2.05	0.96	32	-100.95 ± 18.01	18.5	23.8	...	0	...	0
161001045	2.24 ± 0.23	CPL	373.2 ± 58.6	-0.94	...	2.36 ± 0.19	17.61 ± 1.25	1.01	8	32.57 ± 5.93	20.9	27.7	4-8.727	9.7	...	0
161210524	2.3 ± 2.86	CPL	361.5 ± 106.8	-0.94	...	1.08 ± 0.2	3.9 ± 0.91	0.91	64	24.67 ± 44.67	20.9	27.7	...	0	...	0
170121067	2.3 ± 0.29	CPL	1626 ± 281	-0.75	...	3.68 ± 0.17	10.29 ± 0.87	2.22	8	-6.03 ± 2.1	0.9	6.1	...	0	...	0
170802638	2.24 ± 0.14	CPL	724.1 ± 148.7	-0.81	...	2.6 ± 0.13	37.9 ± 1.6	1.69	8	23.01 ± 10.86	5.4	11	...	0	...	0
170817908	2.62 ± 0.18	CPL	1202 ± 217	-0.93	...	5.44 ± 0.18	10.37 ± 1.61	1.3	8	-21.82 ± 2.12	2.9	25.7	...	0	...	0
180618030	3.71 ± 0.58	CPL	2508 ± 918	-1.13	...	2.15 ± 0.14	14.61 ± 1.86	1.57	8	3.26 ± 10.22	1.5	40.5	...	0	...	0
Group B GRBs																
081107321	1.66 ± 0.23	CPL	70.8 ± 2.3	-0.38	...	1.25 ± 0.04	13.54 ± 0.85	0.47	64	82.84 ± 2.44	62.9	15.6	0.291-10	92.7	0.099-9.909	98
100816026	2.05 ± 0.23	CPL	140.1 ± 6.1	-0.37	...	3.35 ± 0.11	19.88 ± 1.08	1.1	16	137.06 ± 7.38	51.2	17.5	0.318-10	91.6	0.136-7.636	96

Table 2 continued

Table 2 (continued)

GRB	T_{90} (s)	model	E_p (keV)	α	β	$S_{\gamma, -6}$ (erg cm $^{-2}$)	$\dot{\Gamma}_p$ (ph cm $^{-2}$ s $^{-1}$)	HR	res ^a (ms)	τ_{31} (ms)	P_{EP}^b (%)	P_{HR}^b (%)	z_c	P_c^d (%)	z_{EH}^d	P_{EH}^d (%)
101216721	1.92 ± 0.55	CPL	152.9 ± 8.2	-0.86	...	2.92 ± 0.1	25.08 ± 1.84	0.76	16	121.75 ± 7.57	42.7	20.6	0.373-10	89.1	0.182-6.091	92.8
120222021	1.09 ± 0.14	CPL	130 ± 6.9	-0.65	...	1.72 ± 0.06	24.02 ± 1.71	0.76	16	64.52 ± 2.68	14.6	4.3	0.436-10	86	0.327-3.545	78
120323507	0.38 ± 0.04	SBPL	42.2 ± 3.8	-1.17	-2.08	10.7 ± 0.13	603.19 ± 8.22	0.44	4	20.17 ± 0.1	1	0.2	0.046-10	98.4	0.034-10	98.4
140209313	1.41 ± 0.26	Band	143.9 ± 7.5	-0.61	-2.4	9.52 ± 0.18	120.53 ± 3.44	0.93	16	92.03 ± 0.34	24.3	7.7	0.164-10	97	0.086-9.909	98.1
140626843	1.79 ± 1.06	CPL	176.1 ± 22.5	-0.8	...	1.03 ± 0.09	10.06 ± 2.12	0.9	16	887.64 ± 195.02	32.1	15.4	0.891-10	64.2	0.673-1.818	39.3
150923864	1.79 ± 0.09	CPL	143.5 ± 7.6	-0.24	...	1.3 ± 0.05	16.51 ± 1.08	1.1	16	28.76 ± 14.62	40.4	12.3	0.591-10	78.3	0.309-3.727	80
160806584	1.66 ± 0.45	CPL	138.7 ± 9.7	-0.56	...	1.37 ± 0.07	18.53 ± 2.1	0.81	64	191.29 ± 4.39	36.5	13.8	0.545-10	80.6	0.291-3.909	81.8
170206453	1.17 ± 0.1	Band	348 ± 15.2	-0.46	-2.59	10.8 ± 0.16	56.95 ± 2.07	2.12	8	116.86 ± 1.77	3.2	0.8	0.336-10	90.8	0.427-2.545	63.9
171126235	1.47 ± 0.14	SBPL	59.9 ± 7	-0.68	-2.65	2.55 ± 0.09	97.21 ± 6.07	0.12	8	42.06 ± 0.99	51.1	1.1	0.164-10	97	0.055-10	98.3
180511437	1.98 ± 0.97	CPL	107.5 ± 11.9	-0.92	...	0.61 ± 0.04	7.64 ± 1.2	0.51	64	-19.16 ± 44.21	59.8	24	0.691-10	73.4	0.273-4.182	84
180703949	1.54 ± 0.09	CPL	136.9 ± 3	-0.77	...	8.6 ± 0.12	109.24 ± 3.09	0.8	8	62.05 ± 0.49	31.5	11.3	0.182-10	96.5	0.09-10	98.1
Group C GRBs																
081130212	2.24 ± 1	CPL	27.7 ± 2.8	0.45	...	0.21 ± 0.02	11.28 ± 1.75	0.14	128	...	93.4	5.6	0.318-10	91.6	0.057-10	98.3
090320045	2.37 ± 0.27	CPL	304.9 ± 118.2	-1.09	...	0.45 ± 0.11	2.8 ± 0.65	0.92	128	...	28.6	29.2	...	0	...	0
101002279	7.17 ± 2.29	CPL	547.1 ± 210.4	-1.04	...	1.24 ± 0.21	2.87 ± 0.93	0.83	256	-420.61 ± 183.76	76.5	90.8	...	0	...	0
120504945	5.76 ± 0.78	CPL	425.2 ± 79.1	-0.48	...	1.51 ± 0.19	4.98 ± 1.33	2.09	256	760.86 ± 204.07	74.1	55.5	3.364-10	14.4	...	0
131128629	1.98 ± 0.54	CPL	59.2 ± 4.6	0.26	...	0.22 ± 0.02	5.64 ± 1.23	0.39	256	164.35 ± 63	78.7	21.8	0.736-10	71.2	0.2-5.455	90.9
140912664	2.3 ± 1.62	CPL	268 ± 48.5	-0.48	...	0.77 ± 0.13	3.75 ± 0.67	1.75	128	-138.28 ± 91.76	32	10.9	3-10	17.6	...	0
Group D GRBs																
150819440	0.96 ± 0.09	CPL	523.9 ± 34.1	-1.14	...	7.75 ± 0.15	148.44 ± 3.77	0.9	8	1.51 ± 0.01	0.7	2.5	0.682-10	73.8	...	0

^a The time resolution of the lightcurves used to calculate τ_{31} .

^b The probability that GRBs are classified as LGRBs in the E_p - T_{90} plane or the HR - T_{90} plane.

^c The redshift range that GRBs are classified as Type II GRBs in the ϵ - $T_{90,z}$ plane or the EH - $T_{90,z}$ plane. The dotted lines represent that whatever the redshift is, it will not be classified as Type II GRBs.

^d The probability that GRBs are classified as Type II GRBs in the ϵ - $T_{90,z}$ plane or the EH - $T_{90,z}$ plane.